V_2O_5-SiO_2 systems prepared by flame-pyrolysis as catalysts for the oxidative dehydrogenation of propane

I. Rossetti[a], L. Fabbrini[a], N. Ballarini[b], C. Oliva[a], F. Cavani[b], A. Cericola[b], B. Bonelli[c], M. Piumetti [c], E. Garrone[c], H. Dyrbeck[d], E.A. Blekkan[d], L. Forni[a +]

[a]Dip. CFE e ISTM-CNR, Università di Milano, via C.Golgi, 19 20133 Milano (Italy)

[b]Dip. di Chimica Industriale e dei Materiali, Università di Bologna, INSTM, Research Unit of Bologna, NoE Idecat partner (FP6 of EU)

[c]Dipartimento di Scienza dei Materiali ed Ingegneria Chimica, Politecnico di Torino, Torino, Italy, INSTM Unit Torino Politecnico

[d] Department of Chemical Engineering, Norwegian University of Science and Technology, N-7491 Trondheim, Norway

Abstract

VO_x/SiO_2 catalysts have been prepared through an innovative flame-pyrolysis (FP) technique and tested for the oxidative dehydrogenation of propane. The samples, of different V loading, have been characterised by electron paramagnetic resonance (EPR), micro-Raman and FT-IR spectroscopy, to assess the nature of the vanadium active sites in comparison with a sample prepared by impregnation. The active sites of the FP-prepared catalysts showed as highly dispersed $V^{5+}O$ groups, partly incorporated into the silica matrix and poorly interacting with each other. Lower dispersion can be achieved at the same V loading with the catalyst prepared by impregnation. EPR showed $V^{4+}O$ groups pointing out normally from the catalyst surface and sitting in the centre of a surface array of oxygen atoms. These V^{4+} groups helped in marking the difference in catalytic behaviour

of the various samples. Catalytic activity was measured under both aerobic and anaerobic conditions and revealed a promising high selectivity with the FP-prepared samples. The best results were obtained with a 10 wt% V loading, which led to better propylene yield with respect to other samples, especially under anaerobic conditions (up to 80% selectivity at 10% propane conversion). This is very likely related to the much higher dispersion of the VO_x species in the FP-prepared samples, helping also in effectively reducing the coke formation triggered by exposed surface acid sites.

Keywords

Propane ODH; Flame pyrolysis; Silica-supported vanadium; Anaerobic and co-feed reaction conditions.

[+]) Corresponding author, Fax +39-02-50314300, e-mail: lucio.forni@unimi.it

INTRODUCTION

Oxidative dehydrogenation (ODH) of light alkanes offers a potentially attractive route to alkenes, since the overall reaction pathway is exothermic and the thermodynamic constraints of non-oxidative routes are avoided [1-5]. Furthermore, carbon deposition is limited, allowing a more stable catalytic activity. However, the yield of alkenes obtained on most catalysts is lowered by parallel or consecutive reactions, mainly the combustion of reactant and products to CO and CO_2 and the formation of oxygenated by-products, such as acetic acid [6]. In addition to selectivity problems, the co-feeding of oxygen can also bring about safety risks, which can be, however, satisfactorily faced by proper process engineering. On the other hand, selectivity problems can be also partly overcome by optimising the catalyst formulation.

Among the possible active phases, V oxide (VO_x) is the most investigated since, when loaded in proper amount on a suitable support, it leads to promising yields of ethylene [7-10], propylene [6,7,11,12] or butenes [8]. Many different supports have been tested, such as ZrO_2 [13,14], TiO_2 [12], V-substituted zeolites or silicalites [15], SiO_2 [9,13,16] and Al_2O_3, usually as the γ-phase [6-8,10-13,17]. Most investigations deal with the effect of V loading in determining active species distribution and with the role of the support on V surface dispersion. Furthermore, support acidity can negatively affect selectivity when low V loading leaves naked acid sites, mainly in the case of alumina-supported samples [8].

The reaction can be kinetically modelled through a Mars-van Krevelen mechanism centred on V reduction and subsequent reoxidation [6,12]. Indeed, the first reaction step involves V^{5+}, which reduces to V^{4+} and then to V^{3+}. The active oxidised VO_x sites can be promptly restored by oxygen, when co-fed with the paraffin. The nature of such active sites has been widely investigated [13,18,19]. It seems that V^{5+} is dispersed on the support in the form of isolated vanadate species, which progressively oligomerise and polymerise

with increasing V loading until a monolayer is formed. Different V loadings and/or V surface densities corresponding to monolayer formation have been reported, depending on the support and on calcination conditions [10,13,18,20,21]. High activity is ascribed to vanadate species, either isolated or polymerised up to the formation of a VO_x monolayer, while lower activity is usually associated with the presence of bulk V_2O_5. As for selectivity, a possible role of the support cannot be excluded, especially with samples characterised by strong Lewis acidity [11]. In such cases, high selectivity can be achieved when a VO_x monolayer completely covers the support. V loading corresponding to monolayer formation is different for various supports, depending on V-support affinity. It has been shown [13] that samples supported on SiO_2 are mainly constituted by isolated VO_x species up to surface density of *ca*. 2 V/nm^2. When V loading was further increased, V_2O_5 formed, so decreasing catalyst performance. By contrast, alumina- or titania-supported samples showed higher surface density (7-8 V/nm^2), corresponding to polymeric vanadyl species. With the latter supports, it was difficult to attain high V dispersion, unless by excessively decreasing V loading, with a consequent deterioration of catalytic activity.

The catalysts so far described are usually prepared by impregnation, leading to vanadium deposition onto the surface of the selected support. Furthermore, no investigation has been carried out so far, at least to our knowledge, on the possible preparation of nanostructured V-supported catalysts for the present application. A new procedure based on flame-pyrolysis (FP) of an organic solution of metal ion precursors has been set up recently for the preparation of different single or mixed oxides [22-29]. Hence, the catalysts considered in the present paper were prepared by FP, aiming at developing systems in which the active component is dispersed inside the inert matrix, silica in the present case, instead of being deposited over it. The dilution inside porous silica in principle should allow a better dispersion of the active component, so providing also a better control of the heat generated by the reaction and hence a lowering of local

hot spots, that may be detrimental for the process selectivity. A similar result can be achieved by the sol-gel method, that also leads to the incorporation/occlusion of metal oxide nanoparticles inside silica [30] or alumina. However, with respect to the sol-gel method, FP offers the advantage of (*i*) a better control of the preparation procedure and hence of the chemical-physical properties of the final material and (*ii*) a preferred formation of nano-sized agglomerates. Furthermore, the classical preparation procedures for silica (or siliceous materials)-supported vanadium oxide catalysts make use of high-surface-area supports [16,30]. Generally, silica supports possess microporous structure, which make them unsuitable for selective oxidation reactions. By contrast, the FP method usually leads to poorly porous materials having surface area not higher than 150 m^2/g [22-29]. This may represent another advantage of this preparation procedure as compared to conventional techniques.

The aim of the present work was then to prepare by FP a set of nano-structured V-based catalysts characterised by different V loading and to test their performance in ODH of propane in comparison with a sample prepared by impregnating a FP-prepared silica by a traditional procedure. All the samples have been characterised by several physical-chemical techniques and their activity has been tested under different reaction conditions, namely either by co-feeding propane and oxygen or under anaerobic conditions, *i.e.* by simulating an alternate feed of propane and air [17,31-34].

2 – EXPERIMENTAL

2.1 – Catalysts preparation

A detailed description of the FP preparation procedure and of the effect of the main operating parameters on catalyst properties can be found elsewhere [23-26]. Briefly, proper amounts of Vanadium (IV) oxy-acetylacetonate (Merck, 98%) and tetraethyl-orthosilicate (TEOS, Aldrich 99,999 %), were dissolved in an organic solvent (alcohol,

carboxylic acid or a mixture of them), so to obtain a 0.1-0.2 M solution (concentration referred to the nominal oxide composition). The solution was fed (4.4 cm^3/min) to the FP burner, together with 5.0 L/min of oxygen (SIAD, purity >99.95%). The cross section area of the burner nozzle was adjusted so to have a pressure drop of 0.4 bar along it. The main flame was ignited and supported by a ring of twelve premixed O_2 + CH_4 flamelets (CH_4 = 0.5 L/min; O_2 = 1.0 L/min). The catalyst powder so produced was collected by means of a 10 kV electrostatic precipitator [23,35]. The yield was 90-95% for each sample, whose composition is reported in Table 1. The comparative catalyst (V10Si-i, Table 1) was made by impregnation of a FP-prepared SiO_2 batch with NH_4VO_3 solution, followed by drying and calcination at 700°C in air.

2.2 – Catalysts characterisation

Specific surface area (SSA) was measured by N_2 adsorption/desorption at the temperature of liquid nitrogen on a Micromeritics ASAP 2010 apparatus. Microporosity, when relevant, was determined by the *t*-plot procedure. Morphological analysis was done by a LEICA LEO 1430 scanning electron microscope (SEM). XRD analysis was made by a Philips PW1820 powder diffractometer, by using the Ni-filtered Cu Kα radiation (λ=1.5148 Å). The obtained diffractograms were compared with literature data for phase recognition [36]. Thermogravimetric analysis (TGA) of the as-prepared powder was done in flowing air by means of a Perkin-Elmer TGA7 apparatus. Electron paramagnetic resonance (EPR) spectra were collected between -153 and 27°C in air by a Bruker Elexsys instrument, equipped with a standard rectangular ER4102ST cavity and operated at X band, 6.36 mW microwave power and 100 kHz Gauss modulating amplitude. The intensity of the magnetic field was carefully checked with a Bruker ER35M teslameter and the microwave frequency was measured with a HP 5340A frequency meter. Spectral simulations, when required, were done by means of the Bruker SimFonia programme.

Laser-Raman spectra were obtained using a Renishaw 1000 instrument coupled whit a Linkam thermal cell TS 1500; the samples were excited with the 514 nm Ar line under N2 atmosphere. For FT-IR measurements in the low wavenumbers range, powder samples were mixed with optical-grade KBr. For further FT-IR measurements, powder samples were pressed into thin, self-supporting wafers and pre-treated in high vacuum (residual pressure < 10^{-3} mbar) using a standard vacuum frame, in a IR cell equipped with KBr windows. Spectra were collected at 2 cm^{-1} resolution, on a Bruker FTIR Equinox 55 spectrophotometer equipped with MCT detector. To remove moisture and other atmospheric contaminants, the wafers were outgassed for 1 hour at 150, 300 and 500°C before adsorption of CO or NH_3. CO adsorption spectra have been collected at the temperature of liquid nitrogen, by dosing increasing amounts of CO (in the 0.05 – 15.0 mbar equilibrium pressure range) on outgassed samples, inside a special quartz IR cell, allowing simultaneously to dose carbon monoxide and to add liquid N_2. NH_3 has been dosed at r.t., in the 0.01 – 23.0 mbar equilibrium pressure range, followed by removing the reversible fraction of adsorbate by prolonged evacuation. After each experiment, an evacuation step has been performed, to study the reversibility of the interaction.

2.3 – Catalytic activity tests

Catalytic activity was measured by means of a continuous, quartz tubular reactor (i.d.= 7 mm) heated by an electric furnace. The catalyst (0.90 mL, 0.5-0.6 g, 425-600 μm particle size) was activated prior to each run in 20 cm^3/min flowing air, while increasing temperature by 10°C/min up to 550°C, then kept for 1 h. The flow rate of the reactants mixture for the co-feeding mode test was 11 cm^3/min of C_3H_8 (20 mol%) + 11 cm^3/min of O_2 (20 mol%) + 28 cm^3/min of He + 4 cm^3/min of N_2 (60 mol% inert). For the anaerobic mode flow rates were 6 cm^3/min of C_3H_8 (22 mol%) + 19 cm^3/min of He + 2 cm^3/min of N_2. Contact time was 1 s for the former and 2 s for the latter testing mode, respectively. The

exiting gas was analysed by means of a micro-GC (Agilent 3000A), equipped with Plot-Q, OV-1 and MS-5A columns for a complete detection of the effluent products. Propane conversion was calculated as converted over fed propane moles. The selectivity to the *i*-th product was calculated as moles of generated *i*-th species over moles of converted propane, normalized with respect to the reaction stoichiometry. Carbon balance was calculated as the sum of selectivity to the various species.

3 - RESULTS AND DISCUSSION

3.1 – Catalyst preparation and characterisation

Solubility tests showed that the best solvent with fuel properties for the V precursor was ethanol, whereas good miscibility of the Si precursor has been observed with both ethanol and propionic acid. However, by using the latter solvent in 1:1 (vol/vol) ratio with the ethanol solution of V, some problems were encountered at low V loadings ($\leq$10%), in that a much more difficult precursor decomposition in the flame was noticed. This is very likely due to the lower amount of VO_x phase formed, which plays a role in catalysing the oxidation of both the solvent and the organic compounds during synthesis (*vide infra*). Furthermore, a lower flame temperature was attained with the ethanol+propionic acid mixture, thus likely leading to high surface area and low particle size, with respect to the ethanol+1-octanol fuel mixture [26], the latter alcohol being added to increase the combustion enthalpy of the solvent mixture.

During FP a complete combustion of the organic compounds (both solvent and reagents) should be achieved, with the simultaneous formation of the desired oxides. However, some unburnt carbonaceous residua are usually found in the latter. Their amount can be estimated through TGA analysis in flowing air (Table 2). Basically two peaks are observed, one at low temperature (80-170°C), attributed to residual solvent, the

other at higher temperature (500-550°C), attributed to unburnt carbonaceous species. It was observed that at low V content the lower-temperature TGA peak area was comparable to that of the high-temperature peak. Furthermore, the latter shifted towards lower temperature and decreased in intensity with increasing V-loading. This indicates that, during catalyst preparation, the presence of a phase active for oxidation reactions makes precursors decomposition easier. In addition, the samples with low V-loading also showed additional peaks between 150 and 350°C, confirming the difficult decomposition of the precursors.

XRD analysis showed amorphous or sub-microcrystalline powders only and the absence of V-based phases for V loading lower than 28%. A fully reliable V-based phase identification was possible for the sample V50Si only, which showed the V_2O_5 phase reflection peaks [36, file 009-0387]. These results, however, must be compared with those coming from Raman and IR spectroscopy (*vide infra*), able to reveal the presence of vanadia down to a V loading lower than that required by XRD.

SEM pictures (Fig.1) showed a poorly defined morphology for every sample, probably associable with the amorphous structure. However, at high V loading (V50Si) the sample seemed to organise in small spheroidal particles, *ca.* 100 nm in size.

The present results are partly associated with the nature of the selected materials and partly with solvent/fuel choice. Indeed, the use of alcohols did not yield small and homogeneous particle size also for other catalyst compositions [27,28]. However, the increase of particle size uniformity at high V loading seems to confirm the beneficial effect of this element during catalyst preparation.

SSA was minimal for the pure silica support (Table 1), increased with increasing V loading up to 28% V (sample V28Si) and then decreased. Higher SSA are expected when using carboxylic acids, basically because of their decomposition route, involving acids de-carboxylation, with formation of a low-boiling alkane, which allows further fragmentation of

the forming particles during solvent flash [37]. By comparing microporous area, as determined by *t*-plot analysis, with BET SSA (Table 1), one may observe that, in spite of the low surface area of SiO_2, 44% of that value can be ascribed to the contribution of micropores. It should be noticed that in the FP-prepared nanosized samples, microporosity is likely related to inter-particle voids rather than to intra-particle porosity. Upon V addition, micropore surface area progressively decreased with increasing V loading. By keeping in mind the above reported considerations on catalyst morphology, an indirect confirmation of the decrease of particle size can be drawn. Indeed, a slightly higher surface area was obtained with increasing V-loading, though accompanied by a decrease of the contribution of micropores.

3.2 –EPR analysis

The EPR spectral profile of VO_x/SiO_2 samples showed nearly independent of V loading, whereas the spectral intensity increased ca. four times with increasing V concentration from 5% up to 10%. Then, it remained approximately constant at higher V concentration. The most intense EPR pattern, obtained with the V50Si sample, is compared in Fig.2 with the simulation obtained with the parameters reported in Table 3, typical of V^{4+} ions.

With V_2O_5/SiO_2 catalysts EPR spectra of this kind have been attributed [38,39] to V^{4+} species in monolayers and double layers of V_2O_5 supported on SiO_2 in average C_{4v} symmetry. This corresponds to an array of oxygen ligands forming lying parallel to the surface around a V^{4+} - O bond perpendicular to it. The finding that $g_{//} < g_{\perp}$ is attributable to tetragonal distortion. It has been shown [40] that a higher value of the parameter:

$$B = (g_{//} - g_e) / (g_{\perp} - g_e) \qquad (1)$$

indicates a shortening of the V^{4+} - O bond or an increased distance of the oxygen ligands in the basal plane. Both these situations would lead to a strengthening of the V^{4+} - O bond.

In the present case, $B \cong 3.60$ (Table 3) is a value considerably higher than those obtainable with the data elsewhere reported [40] for SiO_2–V^{4+} monolayers (*B* ranging between *ca*. 2.41 and 3.10) and for SiO_2–V^{4+} double layers (*B* ranging between *ca*. 2.24 and 2.65). Therefore, the present relatively high value for *B* indicates that no more than a monolayer of SiO_2–V^{4+} is present on the surface.

Thermal treatment *in vacuo* at 300°C with probable consequent loss of oxygen did not affect significantly the spectral profile and sometimes simply increased a bit its intensity (Fig.3*b*). By contrast, the spectral intensity increased markedly after the catalytic reaction under anaerobic conditions (Fig.3*c*): this can be explained considering that the catalytically active centres are V^{5+}, which reduce during reaction in the absence of co-fed oxygen, leading to an increase of the EPR-active V^{4+} species. Therefore, the latter confirm to represent an intermediate of the catalytic process.

Unlike FP samples, whose EPR spectra are related to isolated V^{4+} species, the spectrum of the V10Si-i sample is composed of three regions (Fig.4), the first contribution (F1) being centred at *ca*. 250 G, the second (F2) at *ca*. 2500 G and the third (F3) at *ca*. 3390 G (corresponding to $g = 1.98$). Bands like these have been attributed [41-45] to ferromagnetic resonance (FMR) of clusters of particles of different shape or size. Systems of this kind were not observed with our FP-prepared samples, in which the V-based active centres were very likely uniformly dispersed and not interacting with each other.

A further paramagnetic contribution P adds to F3 (Fig. 4*a*). Its hyperfine pattern is easily interpreted by subtracting the component *F3* of the spectra of Fig. 4 (*b)* or (*c)* (multiplied by a proper factor) from the spectral region *F3+P of (a)*. By this way, the EPR pattern *P* appears, very similar to that of the FP samples (Fig.2). The only difference is that the value of $g_{//}$ is 1.942, slightly higher than the value of $g_{//} = 1.940$ characterizing the FP-prepared sample. The spectral simulation (not reported) confirms this very small

difference, leading to a value $B \cong 3.5$ for V10Si-i, lower than the value $B = 3.6$ found for V10Si, the former corresponding to a slightly lower V^{4+} - O bond strength in the V10Si-i catalyst.

3.3 - Micro-Raman spectroscopy

Fig.5 reports the Raman spectra of powder samples, in the 200–1200 cm^{-1} range: the inset reports the magnified spectrum of sample V10Si (curve *a*), which shows two weak bands at 1027 and 512 cm^{-1}, readily assigned to isolated V=O species [46]. At higher V loadings (curves *b* and *c*) and with sample V10Si-i (dotted curve *d*), the typical bands of crystalline V_2O_5 are seen, at 285, 304, 404, 482, 525, 701 and 995 cm^{-1} [46-48], whereas no bands were observed on the V5Si sample, with the lowest V content (not reported). As a whole, monovanadates are detected only with sample V10Si, whereas both at higher V loadings and after impregnation, the preferential formation of bulk vanadia occurs.

Possibly formed even with silica supported samples prepared with this new synthetic procedure, oligomeric species would be evidenced by the appearance of Raman bands between 750 e 900 cm^{-1} due to V-O-V stretching in spectra collected on dehydrated samples. By contrast, the band appearing at 1027 cm^{-1} in dehydrated samples and ascribed to V=O is due to both isolated or oligomeric species. Raman spectra of sample V10Si are reported in Fig. 6, where the data were collected with prolonged accumulation to increase signal resolution. Very intense bands due to monomeric species were present and no oligomeric species were observed on both the fresh sample and after dehydration at 200°C. It is interesting to notice that no dramatic change in spectral profile occurred after dehydration.

3.4 - FT-IR analysis: KBr pellets

Fig.7 reports the FT-IR spectra of powders in KBr pellets in the 1500–600 cm^{-1} range, where vibrational modes of the solid absorb: band envelopes *1* (1300–1100 cm^{-1}) and *2* (*ca*. 800 cm^{-1}) are assigned to the asymmetric and symmetric stretch vibrations of Si-O-Si (siloxane) groups of silica, respectively [49]. With all samples, except V10Si-i (curves *a*–*d*), band *3* is seen at 930 cm^{-1}. This band was previously observed in V/Silica and V/Silicalite systems [48,49], *i.e.* amorphous silica and all-silica zeolite incorporating V, and it was assigned to the vibration of SiO_4 groups strongly polarised by the presence of framework vanadium. Such species are not seen with the sample obtained by impregnation (dotted curve *e*), showing that in samples prepared via FP the incorporation of vanadium in the silica framework occurs.

At higher vanadium content (curves *b*–*d*), a component develops at 1010 cm^{-1} (band *4*), assigned [46-48] to crystalline V_2O_5, in agreement with Raman spectra (Fig.5).

3.5 - FT-IR analysis: hydroxyls spectra

Fig.8*a* reports the FT-IR spectra in the hydroxyls range (3800–3100 cm^{-1}) of sample V10Si outgassed at 150, 300 and 500°C. The spectra show a band at 3745–3742 cm^{-1}, assigned to isolated silanols, commonly observed at the surface of amorphous silica [50]. On V10Si outgassed at 150 and 300°C (curves *a* and *b*), the bands of H-bonded silanols are seen as a weak component at about 3720 cm^{-1} (asterisk) and a broad absorption below 3700 cm^{-1}. The former is assigned to terminal silanols of H-bonded SiOH chains, whereas H-bonded silanols inside the chains absorb below 3700 cm^{-1} [50]. After outgassing at 500°C (curve *c*), the band of isolated silanols appears at 3745 cm^{-1}, along with an ill-defined absorption at about 3680 cm^{-1}, which can be due to defective inter-particle silanols [51]. V-OH species, when present, should absorb at about 3675 cm^{-1}, but, due to the abundance of silanols, the corresponding band is probably superimposed to that of H-bonded silanols.

Fig.8*b* shows the FT-IR spectra of samples V10Si, V10Si-i, V5Si and V28Si outgassed at 500°C. The spectra have been normalized to unit specific weight, in order to compare hydroxyls populations of different samples. With V5Si (curve *a*), bands are seen due to free silanols (3745 cm^{-1}) and H-bonded silanols. With respect to V10Si (curve *b*), a higher amount of H-bonded silanols is seen, in agreement with the smaller vanadium content. At higher vanadium content (V28Si, curve *c*), no band is seen at 3745 cm^{-1} and the spectrum becomes very noisy, in agreement with the decreased transparency of the sample, which becomes dark green after outgassing at 500°C. As indicated by Raman spectroscopy data (*vide supra*), the surface of V28Si is covered by V_2O_5, which undergoes reduction by annealing under vacuum at high temperature. The ill-observed broad band is probably due to some surface V-OH species. With V10Si-i (curve *d*), the amount of residual silanols is negligible, probably due to the presence of vanadia, as revealed by Raman spectra.

3.6 - FT-IR analysis: adsorption of NH_3 at r.t and of CO at -196°C

The acidity of surface hydroxyls (isolated and H-bonded silanols, V-OH species) has been analysed by adsorption of basic probes, namely NH_3 and CO. Fig.9 reports the difference spectra recorded after dosage of NH_3 on sample V10Si, outgassed at 150 and 500°C, obtained after subtraction of spectra of the bare sample reported in Fig.8*a*. After ammonia adsorption on V10Si out-gassed at 150°C, a band grows at 1446 cm^{-1}, assigned to the bending vibration of ammonium species formed on Brønsted hydroxyls. At the same time, bands are seen to decrease in the OH stretching region, at 3746, 3675 and 3560 cm^{-1}: the first and the third bands were assigned, respectively, to free and H-bonded silanols, interacting with NH_3, whereas the second band was assigned to V-OH species, more acidic than isolated silanols and therefore responsible of proton transfer to ammonia (1446 cm^{-1}) [52]. After outgassing at 500°C, only the band of isolated silanols is seen to decrease

in the OH stretch range, along with a small component at 3720 cm^{-1}, due to some residual H-bonded silanols (Fig.9*b*): after dehydration, the more acidic hydroxyls (V-OH species and H-bonded silanols) have been removed. At lower wavenumbers, a band is present at 1606 cm^{-1}, assigned to NH_3 coordinated to vanadium ions performing as Lewis acidic sites, now exposed at the surface. The band of ammonium bending vibration is shifted to higher wavenumbers (1465 cm^{-1}), showing that interaction with weaker Brønsted sites (H-bonded silanols absorbing at 3720 cm^{-1}) takes place.

As a whole, different OH species have been observed at the surface of V10Si sample, for which this scale of acidity may be proposed: isolated SiOH < H-bonded SiOH < V-OH. More acidic species, like V-OH, de-hydroxylate first, leaving some Lewis sites accessible to ammonia (band at 1606 cm^{-1}) on the surface.

Fig.10 reports the normalized difference spectra, recorded after dosing *ca*. 0.4 mbar ammonia on different samples outgassed at 500°C. NH_3 does not adsorb on V-10Si-i (curve *a*), in agreement with its low surface area; at higher vanadium content (curves *b* to *d*), the bands of ammonia adsorbed both on Lewis and on Brønsted sites increase in intensity, due to the presence of acidic sites at the catalyst surface.

To assess better the nature of surface hydroxyls, CO adsorption has been studied at the temperature of liquid nitrogen. Fig.11 reports the difference spectra, in the hydroxyls range, obtained after subtraction of that of the bare sample, on sample V10Si out-gassed at 150°C (Section *a*) and 500°C (Section *b*). CO dosage on sample V10Si out-gassed at 150°C (Section *a*) brings about the formation of a broad absorption band below 3600 cm^{-1}, assigned to hydroxyls interacting with CO molecules via H-bonding. The more acidic are the hydroxyls, the larger is the observed shift [53]: species absorbing at 3675 cm^{-1} shift to 3415 cm^{-1} ($\Delta\nu$ = 3675 – 3415 = 260 cm^{-1}), whereas the H-bonded silanols band at 3710 cm^{-1} shifts to 3590 cm^{-1} ($\Delta\nu$ = 120 cm^{-1}), like on silica. When the sample is out-gassed at 500°C (Section *b*), only the features of free silanols (band at 3745 cm^{-1}, shifting to 3645

cm^{-1}, with $\Delta\nu$ = 100 cm^{-1}) and of few residual H-bonded silanols (band at 3710 cm^{-1}, shifting to 3590 cm^{-1}, with $\Delta\nu$ = 120 cm^{-1}) are observed, indicating the preferential elimination of more acidic hydroxyls (V-OH species originally absorbing at 3675 cm^{-1}).

The high concentration of Si-OH groups, and of V-OH as well, notwithstanding the relatively low surface area of the samples, is likely due to the development of a metastable oxide at the high temperature at which the formation of the oxide occurs in the flame. The adopted preparation method leads to materials in which V is partly embedded in the silica matrix and where the rapid dehydration forces the structure to adopt V-O-Si and Si-O-Si strained bonds that are however rapidly hydrolysed during cooling in wet air. This gives rise to V-OH species, with acidity close to that of V-OH found in V/Silicalite [49] and V supported on high surface SiO_2 [48], but formed via a different process. An alternative explanation can be searched in the complex radical reactions taking place into the flame, where OH can attack the V and Si precursors, as well as peroxide radicals which subsequently evolve into the oxide. The intermediate hydroxyl should decompose by dehydration, but this cannot happen if rapid quenching occurs. Similar phenomena have been observed with different materials, which showed residual carbonate species although flame temperature during their synthesis was by far higher than that of carbonate decomposition [24-26]. This would explain the high concentration of hydroxyls in our FP samples and the stabilisation of vanadium into the silica matrix.

3.7 – Catalytic activity

The catalytic activity of all samples has been compared both by co-feeding propane and oxygen (co-feeding mode) and under anaerobic conditions, corresponding to the first step of the cyclic redox-decoupling mode, in which the feed of the hydrocarbon alternates with that of oxygen. The latter procedure allows to alternate reaction and regeneration

steps, so avoiding the co-presence of propane and oxygen. This permits a safer operation and can improve catalyst selectivity to propylene.

a) Anaerobic conditions

Fig.12 *a* and *b* show the performance of the V10Si catalyst, at 550°C, as a function of time-on-stream during the first reduction half-cycle. The initial conversion was close to 14%, but rapidly declined with increasing time-on-stream. Finally, the catalyst attained a steady state, with 6% conversion, due to the dehydrogenation of propane to propylene. Simultaneously, the formation of CO and CO_2 decreased, approaching a value close to zero, while the selectivity to propylene correspondingly increased, from 78% to 90%. Remarkably, neither the selectivity to propylene nor that to CO_x were fully stable after 30 min on-stream, although variations were very small. Therefore, after 30 min the catalysts had not yet totally consumed the bulk oxygen available for the redox reactions. The concentration of H_2 was initially nil, but then increased and reached a value close to 1.8 mol.%.

These results indicate that, at the beginning of the reducing cycle, the catalyst produces propylene through ODH, then progressively shifting to a dehydrogenation (DH) catalyst, when becoming more and more reduced. However, it is important to note that for very small time-on-stream values, when still there is no H_2 production and the catalyst acts as a stoichiometric oxidant, the selectivity to propylene is almost 80%, for a propane 12% conversion. This confirms that the redox-decoupling concept may indeed lead to an effective improvement of selectivity with respect to the co-feed operation (*vide infra*).

Also reported in Fig.12*a* and 12*b* is the catalytic performance for the second reduction half-cycle, *i.e.* after the reoxidation treatment in air at 550°C, following the first cycle. The activity was slightly lower than that observed after the first cycle. This effect can be attributed either to an incomplete reoxidation of the reduced vanadium species, or to an

incomplete removal of coke, or again to some rearrangement of V oxide structure as a consequence of the very exothermal oxidation treatment and of the high local temperature developing on the catalyst surface during this treatment.

Fig.12*c* summarizes the catalytic performance for increasing amounts of vanadium oxide. The progressive reduction of catalyst led to an improvement of selectivity to propylene, due to both a lower consecutive propylene oxidation and an increasing contribution of propane dehydrogenation. The higher the V content, the higher was the propane conversion, both at the very beginning of the reduction step (fully oxidised catalyst) and after 30 minutes on-stream. However, the activity after 30 minutes was not directly proportional to the V content. In fact the conversion achieved with the V50Si sample matched that achieved with V28Si. This effect may be attributed to the value of SSA of the V50Si catalyst, remarkably lower than that of the V28Si sample.

Furthermore, it is worth noting that while V5Si and V10Si allowed a stable performance already after 10 minutes on-stream, V28Si and V50Si were not completely stable even after 30 minutes. This can be attributed to two contrasting factors: (*a*) the progressive migration of bulk O^{2-} towards the surface, still allowing the catalyst to sustain the ODH reaction even after prolonged exposure to the hydrocarbon feed; (*b*) the progressive deactivation, most likely due to coke accumulation, resulting in a decline of the activity of the catalysts.

For all the catalysts the amount of V oxide available for reduction was lower than the theoretical one. Indeed, for V5Si, V10Si and V28Si the experimental weight loss, as calculated from the stoichiometry of reactions involved and from the integral values of propane conversion and selectivity to products, was approximately 25-30% of that calculated for the complete reduction of V^{5+} to V^{3+}. This is likely due to the fact that a fraction of the V oxide was embedded inside the catalyst particles and hence not in contact with the gas phase. Only in the case of the V50Si catalyst the fraction of V oxide that

delivered oxygen attained 70% of the theoretical value. Also for V/Si/O catalysts prepared by the co-gelation procedure [30], less than 50% of V oxide was available for the reaction under anaerobic conditions. It should be noticed that V^{4+} concentration, semiquantitatively calculated from EPR data, seems to increase abruptly from V5Si to V10Si, then levelling off with further increasing of V loading. This can be explained by considering that when V is highly dispersed and incorporated into the silica matrix, it can assume more easily different oxidation states. By contrast, when significant V_2O_5 segregation occurs, a similar concentration of V^{4+} is expected in spite of the increase of V loading.

The hypothesis of coke accumulation on catalyst during the anaerobic operation is supported by several experimental evidences, namely: (*i*) the low final activity of V28Si and V50Si, in line with FT-IR data on NH_3 and CO adsorption (*vide supra*) (*ii*) the experimental trend for H_2 formation (*vide infra*); (*iii*) the selectivity to propylene (close to 75%) after prolonged exposure to the hydrocarbon feed, lower than that (90-95%) obtained with V10Si (although comparable to that of V5Si). The lower selectivity to the olefin was due to the poorer C balance, in average between 80 and 85% for V28Si and V50Si, but close to 95% (Fig.12*a*) for V10Si. This is an indication of the accumulation of coke on the catalyst surface. It is worth noting that also in the case of V5Si the average C balance in the 20-to-30 minutes on-stream range was close to 85% and the selectivity to propylene was close to 75%. This indicates that under anaerobic conditions the accumulation of coke is favoured with catalysts containing the lowest (V5Si) and the highest (V28Si and V50Si) amount of vanadium oxide, showing a relevant role played by the support acidity in promoting coke formation with V5Si and by the acidity of the V sites with high degree of aggregation (*i.e.,* in bulk vanadium oxide) with V28Si and V50Si.

Further evidences for the formation of coke under anaerobic conditions can be seen in Raman spectra of spent catalysts (*i.e*. analysed after the reducing step). The typical Raman features associated to the presence of coke have been observed (Fig. 13).

Furthermore, during the half-cycle reoxidation step of the reduced catalyst, the formation of CO_2 was observed, together with minor amounts of CO. The formation of these compounds was maximal during the first 8-10 minutes of treatment, then becoming practically nil after approximately 15 minutes.

When taking into consideration the initial performance, the high activity of V28Si and V50Si also corresponds to a lower selectivity to propylene. This is the consequence of the higher alkane conversion and of the greater degree of V aggregation, both favouring the consecutive reaction of propylene combustion. The higher initial selectivity was shown by the V5Si and V10Si catalysts. The former sample, however, showed a decline of selectivity after the initial period. V10Si thus seems to represent the best compromise between the need to expose as much as possible the active component at the catalyst surface and to keep a high degree of V oxide dispersion.

In addition, in order to compare the performance of the differently loaded materials (strongly differing in their activity) at similar degree of conversion and at similar degree of reduction level, we carried out tests with the V10Si catalyst at gas contact time of 4 s (Fig. 12*c*). Under these conditions, the fully oxidized V10Si catalyst allowed 23% propane conversion, with selectivity to propylene of 66%. This result can be compared with the performance of the fully oxidized V28Si catalyst, which allowed 30% propane conversion and 33% selectivity to propylene at 2 s gas contact time. It is evident that the V10Si catalyst, that does not contain bulk vanadium oxide, is more selective to propylene than V28Si, which contains a certain amount of bulk vanadium oxide (as determined by spectroscopic analyses, such as Raman).

The observed H_2 formation (Fig.14*a*) was close to zero for all catalysts at the beginning of the reaction and then progressively increased. The amount of hydrogen produced was greater for samples with higher V oxide content, in agreement with the higher activity in propane DH (Fig.12*c*). However, while with V5Si and V10Si the formation

of hydrogen remained constant after 10 minutes on-stream, with V28Si and especially with V50Si the formation of H_2 reached a maximum at *ca.* 15 minutes on-stream. This was clearly due to coke accumulation. However, it is worth noting that in the case of V28Si and V50Si the amount of H_2 produced was much greater than that corresponding to propylene formation, *i.e.* 2.7% *vs*. a theoretical 1.6 mol% for V28Si and 2.7% *vs*. a theoretical 1.4 mol% for V50Si, after 30 minutes on-stream. The difference is even much greater, especially with V50Si, when considering the maximum concentration of H_2 at 15 min on-stream. This means that an additional contribution to H_2 formation exists, besides propane DH. The relative importance of this further reaction increases when the amount of V oxide loading increases. The additional contribution to H_2 evolution may come from coke formation, which on the other hand decreases the instantaneous propane conversion and hence the total amount of H_2 produced at higher time-on-stream values.

Finally, Fig.14*b* compares the selectivity *vs*. conversion for all the present catalysts, under anaerobic conditions. Although the plot may be somehow misleading, due to the fact that for a given level of conversion the catalysts had been exposed to the reducing stream for different times, and hence they possess different oxidation levels, nevertheless the results confirm the better selectivity to propylene achieved with V10Si. For the latter catalyst, the Figure reports also the previously mentioned activity data at gas contact time of 4 s.

b) Co-feed conditions

Fig.15*a* and 15*b* summarise the performance of the V10Si sample under co-feed conditions. Total O_2 conversion is reached already at 450°C, with a corresponding 26% propane conversion. An increase of temperature leads to a further increase of propane conversion, mainly because of the additional contribution of propane dehydrogenation. Selectivity to propylene is good (75%) only for very low propane conversion (less than

1%), but it decreases when reaction temperature and propane conversion increase. Above 480°C, however, the contribution of propane dehydrogenation (as evident from the formation of molecular hydrogen) leads to a better selectivity to propylene and to a lower selectivity to CO and CO_2. This catalyst showed the best selectivity also under co-feed conditions (*vide supra*).

In addition to a higher activity, due to the higher V-loading (*vide infra*), with V50Si (Fig.15*a* and 15*c*), the main difference concerns selectivity to CO and CO_2 at high temperature. It can be noticed that, despite the total O_2 conversion had already been reached around 350°C, a further increase of temperature led to an increase of selectivity to CO_2 and to a decrease of that to CO. In a previous work [54] this was attributed to the activity of reduced bulk vanadium oxides, which catalyse the water gas shift (WGS) reaction. Another difference concerns the remarkable selectivity to acetic acid. In ref. 54, when the loading of V oxide, over either silica or alumina, was lower or close to the theoretical monolayer, the catalysts did not exhibit any activity for the WGS reaction. The same occurs with the present catalysts.

Fig.16*a* and 16*b* compare propane conversion and selectivity to propylene as a function of reaction temperature for all catalysts (tests were run before the anaerobic tests). Activity is proportional to the V content. The best selectivity to propylene was obtained also here with the V10Si catalyst. The catalyst having the lowest V content (V5Si) was totally unselective to propylene at low conversion, forming almost exclusively CO_2. Both V28Si and V50Si were less selective to propylene than V10Si. For all catalysts, in the low temperature range selectivity decreased when propane conversion increased, due to the contribution of the consecutive reaction of propylene combustion. An increase of selectivity was observed after attaining total oxygen conversion, due to the increased contribution of propane dehydrogenation. It is evident that the catalytic performance of these silica-based materials is worse than that of other siliceous materials (MCF or MCM-

41), in which V incorporation or grafting, aimed at obtaining very disperse (isolated) species, led to samples having surprisingly high selectivity and productivity to the olefin [55]. The same authors pointed out that the latter samples offer a much better performance than catalysts prepared by conventional impregnation of vanadium oxide over silica.

c) Comparison between FP-prepared and impregnated catalysts

Fig.17 compares the performance under anaerobic conditions of V10Si and of the reference catalyst V10Si-i, obtained by impregnation of the FP-prepared silica. The V oxide should be prevalently dispersed over the silica surface with V10Si-i, predominantly in the form of bulk vanadia aggregates, as shown in the characterisation section. By contrast, though the same total amount of vanadium is present in both samples, it should be at least in part embedded in the bulk with V10Si sample. The two samples showed quite comparable initial activity, notwithstanding the remarkably higher value of SSA of the FP-prepared sample, with respect to that of V10Si-i. This is probably due to the fact that the available amount of V oxide is higher with the V10Si-i catalyst (being it deposited over silica), than with the FP-prepared catalyst. In fact, with the V10Si-i catalyst, the weight loss, calculated from the stoichiometry of the reactions occurring under anaerobic conditions, corresponds to approximately 50% of the theoretical value (calculated by assuming a complete reduction of V_2O_5 into V_2O_3) and is almost two times higher than the weight loss found for the V10Si catalyst.

Propane conversion followed the same trend for the two catalysts (Fig.17*a*), but the selectivity (Fig.17*b*) achieved with the FP-prepared catalyst was clearly better than with the impregnated one. The difference in selectivity is evident at the beginning of the reducing period, when the catalyst is still fully oxidised, then diminishing as long as the catalyst progressively reduces. The difference at the beginning of the reducing period confirms the different nature of the V species responsible of the ODH of propane.

In the same Figure the behaviour of catalyst V28Si is also reported. This sample showed the presence of crystalline V_2O_5 and showed an overall amount of vanadium oxide available for reaction (as measured from the comparison between the theoretical weight loss and the experimental one in anaerobic tests) of approx 8 wt%, not far from that (5 wt%) of V10Si-i catalyst. Sample V28Si was not only more active, but also clearly more selective than V10Si-i. This is a further evidence of the better performance of the catalysts prepared by the FP method.

d) Comparison between anaerobic and co-feed reaction conditions

Finally, Fig.18 compares the selectivity to propylene *vs.* propane conversion under co-feed and under anaerobic conditions. It is worth mentioning that in the former case the conversion was varied by changing temperature, whereas under reducing conditions the conversion progressively changed during the permanence at isothermal conditions (T=550°C) in the reducing stream. Therefore, the most significant comparison is that made for the still oxidized catalysts, *i.e.* at the very beginning of the reducing time. This corresponds, for each catalyst, to the highest instantaneous conversion of propane. The comparison clearly evidences that the operation under anaerobic conditions may provide advantages in terms of selectivity, with respect to the co-feed operation. Specifically, while in the case of V28Si and V50Si the selectivity to propylene achieved in the presence and in the absence of oxygen (in the latter case, for the fully oxidized catalyst) were not much different, in the case of V5Si and V10Si a remarkably higher selectivity was obtained under anaerobic conditions. Especially with the latter catalyst, selectivity to propylene at the beginning of the reducing time, at *ca*. 15% conversion, was by more than 60% higher than that obtained in the presence of oxygen at comparable propane conversion. In fact, Fig.15*a* and 15*b* show that, between 450 and 475°C, in the co-feed mode propane conversion increased from 7 to 27%, oxygen conversion from 20% to 98%, and selectivity

to propylene decreased from 22 to 17%. The latter is considerably lower than that obtained with the V10Si sample in the absence of molecular oxygen.

In a previous work on V_2O_5-SiO_2 catalysts with VO_x dispersed in the gel [30], the reaction under anaerobic conditions led to an effective improvement of selectivity to propylene (around 25-30 points% higher for a 35-40% propane conversion) with respect to the co-feed conditions. The best selectivity was achieved at the very beginning of the reducing step, when the catalyst was still fully oxidised and acted as a true ODH catalyst even in the absence of molecular oxygen. Remarkably, this property was specific of the V_2O_5-SiO_2 system. In fact, when vanadium oxide was supported over either alumina or titania, no effective improvement in propylene selectivity was observed for the anaerobic operation with respect to the co-feed mode [17].

In the present investigation, the best performance in propane ODH under both co-feed and anaerobic conditions was observed with the catalyst containing 10 wt% V_2O_5. Only VO_x isolated species and no vanadium-oxide aggregates were present in this catalyst, as observed by Raman spectra (*vide supra*). This is an advantage brought about by the FP preparation technique, which allows higher V loading before V_2O_5 starts segregating. By contrast, when silica is used as support, the amount of vanadium oxide is higher than that required for monolayer formation, leading to V_2O_5 formation at V loading lower than with the present FP-prepared samples. This is likely due to the peculiarity of the latter samples, which exhibit a surface concentration of Si-OH much higher than expected and decreasing when increasing the V loading, as shown by FT-IR data (*vide supra*). Furthermore, as evidenced by the spectroscopic characterisation, the development of V-O-Si bonds confirms that a prerequisite for the formation of isolated VO_x species is the presence of a high concentration of surface hydroxyl groups. It can be hypothesised that, after the high-temperature flash vaporisation and pyrolysis of the precursors organic solution in the flame, the development of a metastable oxide is followed by the opening of

strained Me-O-Me bonds and generation of Me-OH moieties during the quenching in the wet atmosphere. On the other hand, the FP method favours the formation of V-O-Si bonds and hence the generation of a concentration of isolated VO_x species greater than that usually obtained with impregnated silica. The successive calcination treatment at 550°C may further favour the development of additional V-O-Si bonds and the generation of isolated VO_x species. This also occurred with the V5Si catalyst, in which however a greater fraction of exposed silica caused a worsening of performance and a lower selectivity to propylene, due to a more abundant formation of carbon oxides under the co-feed mode and of coke under anaerobic conditions. In contrast, with the samples V28Si and V50Si, the characterisation clearly showed the formation of bulk vanadia aggregates. The latter are responsible for the formation of carbon oxides and acetic acid in the co-feed mode and of carbon oxides under anaerobic reaction conditions.

The comparison between the catalyst prepared with the sol-gel method and containing 7 wt% V2O5 [30] and catalyst V10Si reported in the present work evidences that the two samples behave similarly under anaerobic conditions (very similar plots of selectivity to propylene as a function of conversion), but the sol-gel catalyst gives a better selectivity than the FP catalyst under co-feed conditions. This difference can be attributed to the greater exposure of V-OH and Si-OH groups for the FP-prepared catalyst. However, under anaerobic conditions the V10Si catalyst leads to a much greater enhancement of selectivity to propylene than the corresponding sol-gel catalyst. This means that the hydroxyl groups do not play a negative role on selectivity when the reaction is carried out in the absence of molecular oxygen.

The present results confirm a substantial difference in the nature of V sites of the FP-prepared samples with respect to the impregnated one and to those prepared by conventional techniques, such as sol-gel [30]. Indeed, high V dispersion is evident for the FP-prepared samples, at least up to 10 wt% V_2O_5. No segregated vanadia can be seen in

catalyst V10Si by either XRD, or Raman, or FT-IR analysis. Furthermore, no V^{4+} ferromagnetic domains are evidenced by EPR spectroscopy, in contrast to the V10Si-i sample (Fig.4). In addition, the EPR results can be helpful for enlighting the local structure of the V-based active sites. Indeed, the EPR features due to V^{4+} keep constant their profile, but grow markedly in intensity after reaction under anaerobic conditions (Fig.3), indicating not only that a considerable amount of V^{4+}-based species form upon reduction of V^{5+} during the catalytic process, without re-oxidation, but also that in these species the V^{4+} - O bond is a bit stronger in the V10Si than in V10Si-i sample (*vide supra*). This suggests that the bonds forming between surface V and O is stronger in the former than in the latter sample very likely also in the V^{5+} active centres. This is in agreement with the observed activity data, as samples with stronger V^{4+} to O bonds were characterized by lower oxygen availability, *i.e.* by lower activity, but higher selectivity.

The comparison of the V10Si and V10Si-i catalysts gave also additional indications. The two samples yielded very similar performance in the co-feed mode, but the V10Si sample gave a higher selectivity to propylene under anaerobic conditions. Since the activity of the two catalysts was very similar, this difference is attributable to the different nature of VO_x species. Noteworthy, IR bands due to vibration of SiO_4 groups perturbed by the presence of neighbouring V ions were not observed in the case of the V10Si-i sample. Therefore, it is a peculiarity of the FP method, involving the concomitant flame pyrolysis of the V-Si complex species, to cause the partial incorporation of V ions in silica. The hydrolysis of surface Me-O-Me strained bonds may lead to the exposure of sub-surface VO_x species. These species are located in a nest surrounded by Si-OH species, which also contribute to the isolation of the V ion. The presence of a greater concentration of isolated VO_x species in V10Si with respect to V10Si-i showed a positive effect on selectivity to propylene, but only when the reaction was carried out under anaerobic conditions. The same was observed in the case of V_2O_5/SiO_2 cogel systems [30] and was

attributed to the fact that, when the reaction is carried out in the presence of molecular oxygen, the generation of unselective O^{2-} species, rather than the dispersion of the active sites, controls the selectivity of the process. When instead the reaction is carried out in the absence of molecular oxygen, a better isolation of the active sites may effectively control the availability of surface O^{2-} sites and hence limit the consecutive and parallel total combustion reactions.

Fig.18 shows that the V10Si-i catalyst gave a better selectivity to propylene under anaerobic conditions than in the co-feed mode. The gain in selectivity was around 25-30 points % at 15-20% propane conversion. However, the same Figure also shows that the improvement in selectivity achieved with the V10Si catalyst was considerably higher, by *ca.* 50-60 points %. It is evident that the concomitant generation of the V and Si oxides achieved by the FP method generates a system that provides a superior performance under anaerobic conditions, because of the development of a greater concentration of isolated VO_x sites.

4 - Conclusions

VO_x/SiO_2 catalysts with different V loading have been prepared by flame pyrolysis. Their physical-chemical and catalytic properties for the ODH of propane appeared markedly different from those of a comparative sample prepared by impregnation. Indeed, much higher V dispersion has been achieved for the FP-prepared sample with respect to the impregnated catalyst at the same V loading. Higher selectivity to propylene has been achieved with the present FP-samples, especially under anaerobic conditions. The active sites of the FP-prepared catalysts showed to be highly dispersed $V^{5+}O$ groups, partly incorporated into the silica matrix and poorly interacting with each other. EPR characterisation allowed to elucidate V^{4+} sites structure, consisting in $V^{4+}O$ groups sitting in the centre of a surface array of oxygen atoms. High V site isolation was evidenced

especially for the FP-samples up to 10 wt% V loading, together with the absence of oligomeric species. However, for higher V-loading, bulk vanadia started segregating, with a consequent lowering of catalyst selectivity. The unexpectedly high surface hydroxyls concentration detected on the FP samples, in spite of the high calcination temperature attained during the synthesis, very likely helps stabilising these dispersed V species. Hence, the advantage of the present FP-preparation method, with respect to other preparation procedures, is the possibility to host higher V concentration without V_2O_5 segregation, so permitting higher selectivity with respect to that provided by traditionally prepared catalysts.

ACKNOWLEDGEMENTS

We are grateful to: MUR (Italian Ministry of University and Research) for financial support through the COFIN programme, prot.2005038244; INSTM for a PhD grant to A. C.; the Norwegian Research Council for the PhD grant and travel grant for H. D. through the KOSK programme; S. Cappelli for EPR spectra collection.

REFERENCES

1 - F. Cavani, F. Trifirò, Catal. Today 24 (1995) 307.

2 - E.A. Mamedov, V. Cortes-Corberan, Appl. Catal. A 127 (1995) 1.

3 - T. Blasco, J.M. Lopez Nieto, Appl. Catal. A 157 (1997) 117.

4 - F. Cavani, F. Trifirò, in “Basic Principles in Applied Catalysis”, M. Baerns (Ed.), Springer, Berlin, Series in Chemical Physics 75 (2003) p. 21.

5 - N. Ballarini, F. Cavani, A. Cericola, Catal. Today 127 (2007) 113.

6 - A. Bottino, G. Capannelli, A. Comite, S. Storace, R. Di Felice, Chem. Eng. J., 94 (2003) 11.

7 - M.D. Argyle, K. Chen, A.T. Bell, E. Iglesia, J. Catal., 208 (2002) 139.

8 - T. Blasco, A. Galli, J. M. Lòpez Nieto, F. Trifirò, J. Catal., 169 (1997) 203.

9 - Z. Zhao, Y. Yamada, A. Ueda, H. Sakurai, T. Kobayashi, Catal. Today, 93–95 (2004) 163.

10 – M.V. Martìnez-Huerta, X. Gao, H. Tian, I.E. Wachs, J.L.G. Fierro, M.A. Bañares, Catal. Today, 118 (2006) 279.

11 - E.V. Kondratenko, N. Steinfeldt, M. Baerns, Phys. Chem. Chem. Phys., 8 (2006) 1624.

12 - D. Shee, T.V. Malleswara Rao, G. Deo, Catal. Today, 118 (2006) 288.

13 - H. Tian, E.I. Ross, I.E. Wachs, J. Phys. Chem. B, 110 (19) (2006) 9593.

14 - K. Chen, E. Iglesia, A. T. Bell, J. Catal., 192 (2000) 197.

15 – S. Dz´wigaj, I. Gressel, B. Grzybowska, K. Samson, Catal. Today, 114 (2006) 237.

16 - N. Ballarini, A. Battisti, F. Cavani, A. Cericola, C. Lucarelli, S. Racioppi, P. Arpentinier, Catal. Today, 116 (2006) 313.

17 - N. Ballarini, F. Cavani, A. Cericola, C. Cortelli, M. Ferrari, F. Trifirò, G. Capannelli, A. Comite, R. Catani, U. Cornaro, Catal. Today 91-92 (2004) 99.

18 – M.D. Argyle, K. Chen, C. Resini, C. Krebs, A.T. Bell, E. Iglesia, J. Phys. Chem. B, 108 (2004) 2345.

19 – N. Steinfeldt, D. Müller, H. Berndt, Appl. Catal. A: General, 272 (2004) 201.

20 - X. Gao, S.R. Bare, J.L.G. Fierro, I.E. Wachs, J. Phys. Chem. B, 103 (1999) 618.

21 - X. Gao, J.L.G. Fierro, I.E. Wachs, Langmuir,15 (1999) 3169.

22 - W.J. Stark, L. Mädler, S.E. Pratsinis, EP 1,378,489 A1 (2004), to ETH, Zurich.

23 - G.L. Chiarello, I. Rossetti, L. Forni, J. Catal., 236 (2005) 251.

24 – G.L. Chiarello, I. Rossetti, P. Lopinto, G. Migliavacca, L. Forni, Catal Today, 117 (2006) 549.

25 - G.L. Chiarello, I. Rossetti, L. Forni, P. Lopinto, G. Migliavacca, Appl. Catal. B: Environmental, 72 (2007) 218.

26 - G.L. Chiarello, I. Rossetti, L. Forni, P. Lopinto, G. Migliavacca, Appl. Catal. B: Environmental, 72 (2007) 227.

27 - R. Strobel, W.J. Stark, L. Mädler, S.E. Pratsinis, A. Baiker, J. Catal., 213 (2003) 296.

28 - L. Mädler, S.E. Pratsinis, J. Am. Ceram. Soc., 85 (7) (2002) 1713.

29 - R. Strobel, S.E. Pratsinis, A. Baiker, J. Mater. Chem., 15 (2005) 605.

30 - N. Ballarini, F. Cavani, M. Ferrari, R. Catani, U. Cornaro, J. Catal., 213 (2003) 95.

31 - R. Grabowski, S. Pietrzyk, J. Słoczynski, F. Genser, K. Wcisło, B. Grzybowska-Swierkosz, Appl. Catal. A 232 (2002) 277.

32 - G.E. Vrieland, C.B. Murchison, Appl. Catal. A 134 (1996) 101.

33 - D. Creaser, B. Andersson, R.R. Hudgins, P.L. Silveston, Chem. Eng. Sci. 54 (1999) 4365.

34 - D. Creaser, B. Andersson, R.R. Hudgins, P.L. Silveston, J. Catal. 182 (1999) 264.

35 - R. A. M. Giacomuzzi, M. Portinari, I. Rossetti, L. Forni, Stud. Surf. Sci. And Catal., A. Corma, F.V. Melo, S. Mendioroz, J.L.G. Fierro, Eds., Vol. 130, Elsevier, Amsterdam, 2000, p.197.

36 - Advanced Selected Powder Diffraction Data, Miner. DBM (1–40), J.C.P.D.S., Swarthmore, PA, 1974–1992.

37 - W.J. Stark, L. Mädler, M. Maciejewski, S.E. Pratsinis, A. Baiker, Chem. Comm., (2003) 588.

38 - V.K. Sharma, A. Wokaun, A. Baiker, J. Phys. Chem., 90 (1986) 2715.

39 - A. Gervasini, G. Fornasari, G. Bellussi, Appl. Catal. A: General, 83 (1992) 235.

40 - E.G. Derouane, A.J. Simoens, J.C. Védrine, Chem.Phys.Lett., 52 (1977) 549.

41 - E.G. Derouane, A. Simoens, C. Colin, G.A. Martin, J.A. Dalmon, J.C. Védrine, J. Catal., 52 (1978) 50.

42 - P.A. Jacobs, H. Nijs, J. Verdonck, E.G. Derouane, J.-P. Gilson, A.J. Simoens, J.Chem.Soc. Faraday Trans. I, 75 (1979) 1196.

43 - C. Kittel, “Introduction to Solid State Physics”, J.Wiley, New York, 1967, 3rd Edition, p. 523.

44 - L. Bonneviot, D. Olivier, “Ferromagnetic Resonance”, in “Catalyst Characterization. Physical Techniques for Solid Materials”, B. Imelik, J.C. Védrine, Eds., Plenum Press, New York, 1994.

45 - T. Ono, H. Numata, J. Molec. Cat. A: Chemical, 116 (1997) 421.

46 - A. Khodakov, B. Olthof, A.T. Bell, E. Iglesia, J. Catal. 181 (1999) 205 and references therein.

47 – A. Klisińska, S. Loridant, B. Grzybowska, J. Stoch, I. Gressel, Applied Catal. A: General 309 (2006) 17.

48 – D.E. Keller, T. Visser, F. Soulimani, D.C. Koninsberger, B.M. Weckhuysen, Vibrational Spectroscopy 43 (2007) 140.

49 – S. Dzigwaj, P. Massiani, A. Davidson, M. Che, J. Molec. Cat. A: Chemical, 155 (2000) 169.

50- A. Burneau, J.P.Gallas, The Surface Properties of Silica, A.P. Legrand, Ed., 1999, 194 and references therein.

51 – B.A. Morrow, A.J. McFarlan, J. Phys. Chem. 96 (1992) 1395.

52- J.A. Lercher, C. Gründling, G. Eder-Mirth, Catal. Today, 27 (1996) 353.

53. A. Zecchina, C. Otero Areán, Chem. Soc. Rev. 25 (1996) 187.

54 - N. Ballarini, A. Battisti, F. Cavani, A. Cericola, C. Cortelli, M. Ferrari, F. Trifirò, P. Arpentinier, Appl. Catal. A: General, 307 (2006) 148.

55 - Y.-M. Liu, W.-L. Feng, T.-C. Li, H.-Y. He, W.-L. Dai, W. Huang, Y. Cao, K.-N. Fan, J. Catal. 239 (2006) 125.

Table 1: Composition and SSA of the prepared catalysts. Values in parentheses represent SSA due to micropores contribution as determined by *t*-plot

Sample	$V_2O_5/(V_2O_5+SiO_2)$ wt%	SSA (m^2/g)
SiO_2	-	14 (6)
V5Si	5.0	41 (14)
V10Si	10.0	75 (n.d.)
V28Si	28.4	80 (n.d.)
V50Si	50.0	46 (8.6)
V10Si-i*	10.0	-

* Prepared by impregnation of the FP-prepared support

Table 2: Weight loss during TGA analysis and temperature of the main peaks observed

Sample	**1st peak T (°C)**	**2nd peak T (°C)**	**Total wt% loss**	**2nd peak wt% loss**
SiO_2	80	515	3.7	1.7
V5Si	170	550	6.3	1.4
V10Si	170	520	2.9	0.7
V28Si	90	520	7.8	1.0
V50Si	105	495	5.5	0.3

Table 3: EPR experimental parameters

	$g_{//}$	$g_{\perp}$	***B* (*)**	$A_{//}$ **/G**	$A_{\perp}$ **/G**	$\Delta W_{//}$ **/G (°)**	$\Delta W_{\perp}$ **/G (°)**
V10Si	1.940	1.985	3.60	194	77	20	15
V10Si-i	1.942	1.985	3.50	194	77	20	15

(*) From Eq.(1); (°) Lorentzian-shaped line width

FIGURE CAPTIONS

Figure 1: SEM micrographs of the prepared samples. Marker size: 500 nm except for V28Si (1 μm).

Figure 2: : EPR spectrum of sample V50Si. Upper track, experimental; lower track, computer simulation with the spectral parameters reported in Table 3 and corresponding to isolated (monovadates) $V^{4+}Ox$ species.

Figure 3: EPR spectra at r.t. of sample V28Si: (*a*) as prepared, (*b*) after deoxygenation, (*c*) after catalytic use under anaerobic conditions and deoxygenation.

Figure 4: EPR spectra of sample V10Si-i at (*a*) -154 °C, (*b*) 25°C and (*c*) 127°C. F1, F2 and F3 indicate ferromagnetic resonance features.

Figure 5: Raman spectra, in the 200 – 1200 cm^{-1} range, recorded with samples V10Si, V28Si, V50Si and V10Si-i (curves *a, b, c* and *d*, respectively). Inset to Figure: magnification of curve *a* (V10Si).

Figure 6: Raman spectra of sample V10Si (prolonged acquisition time). Comparison between the fresh sample and after dehydration at 200°C.

Figure 7: FT-IR spectra, in the 1500–600 cm^{-1} range of samples V5Si, V10Si, V28Si, V50Si and V10Si-i (curves *a, b, c, d* and *e*, respectively) in KBr pellets.

Figure 8: Section *a*: FT-IR spectra, in the 3800–3000 cm-1 range, of sample V10Si outgassed at 150 (curve *a*), 300 (curve *b*) and 500°C (curve *c*). Section *b*: Normalized FT-IR spectra, in the 3800–3000 cm^{-1} range, of samples V5Si (curve *a*), V10Si (curve *b*), V28Si (curve *c*) and V10Si-i (curve *d*) out gassed at 500°C.

Figure 9: FT-IR difference spectra recorded after dosing NH_3 at r.t. on sample V10Si out gassed at 150°C (Section *a*) and 500°C (Section *b*). NH_3 partial pressures in the 0.01 – 23.0 mbar range. Bold curves: spectra recorded after 30 min out gassing at r.t.

Figure 10: Normalized FT-IR difference spectra recorded after dosing 0.4 mbar of NH_3 at r.t. on samples V10Si-i (curve *a*); V5Si (curve *b*); V10Si (curve *c*) and V28Si (curve *d*).

Figure 11: FT-IR difference spectra recorded after dosing CO at the temperature of liquid N_2 on sample V10Si out gassed at 150°C (Section *a*) and 500°C (Section *b*). CO partial pressures in the 0.05–15.0 mbar range.

Figure 12: Effect of time on-stream during the anaerobic reducing step (half-cycle) over catalyst V10Si on: *a*) propane conversion (◆) and atomic % C balance (▲) during the first reducing half-cycle, and propane conversion during the second reducing half-cycle (◇) for catalyst V10Si; *b*) molar selectivity to propylene (■), carbon monoxide (◆), carbon dioxide (▲), light hydrocarbons (●),out coming H_2 concentration (mol %) (△) and selectivity to propylene during the second reducing half-cycle (□). *c*) Propane conversion (full symbols) and molar selectivity to propylene (open symbols), for catalysts V5Si (◆,◇), V10Si (▲,△), V28Si (■,□) and V50Si (●,○). T 550°C, gas contact time 2 s. Propane conversion (∗) and molar selectivity to propylene (×) for catalyst V10Si at 550°C and gas contact time 4 s.

Figure 13: Raman spectra of V28Si, fresh sample and after run under anaerobic conditions.

Figure 14: Effect of time on-stream on: *a*) hydrogen concentration in the out coming stream and *b*) propylene molar selectivity *vs* conversion, during the anaerobic reducing step (half-cycle) for catalysts V5Si (◇), V10Si (△= gas contact time 2 s, ▲= gas contact time 4 s), V28Si (□) and V50Si (○). T 550°C, gas contact time 2 s.

Figure 15: Effect of reaction temperature: *a*) on propane (◆) and oxygen (■) conversion in the co-feed mode over catalysts V10Si (full symbols), and V50Si (empty symbols); *b*) on molar selectivity to propylene (■),carbon monoxide (◆), carbon dioxide (▲), light hydrocarbons (●), acetic acid (○) and to the outlet H_2 mol % concentration (□) in the co-feed mode over catalyst V10Si. *c*) As for *b*) but over catalyst V50Si.

Figure 16: Effect of reaction temperature *a*) on propane conversion and *b*) on molar selectivity to propylene. Co-feed mode, catalysts V5Si (◆), V10Si (▲), V28Si (■), V50Si (●) and V10Si-i (□).

Figure 17: *a*) Effect of time on-stream during the anaerobic reducing step (half-cycle) on propane conversion. *b*) Molar selectivity to propylene *vs*. propane conversion, for V10Si (■) V10Si-i (□) and V28Si (◆) catalysts at T=550°C.

Figure 18: Molar selectivity to propylene *vs* propane conversion for the anaerobic (full symbols) and co-feed (open symbols) modes. Catalysts V5Si (◆,◇), V10Si (▲,△), V28Si (■,□), V50Si (●,○) and V10Si-i (∗,×). T 550°C, gas contact time 2 s.

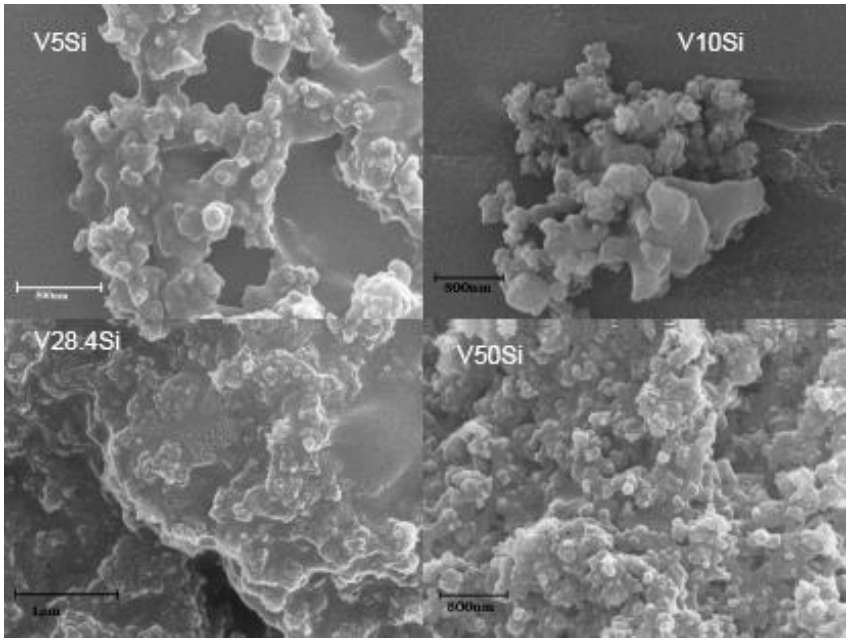

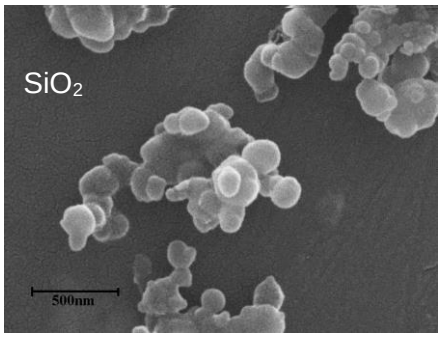

Figure 1

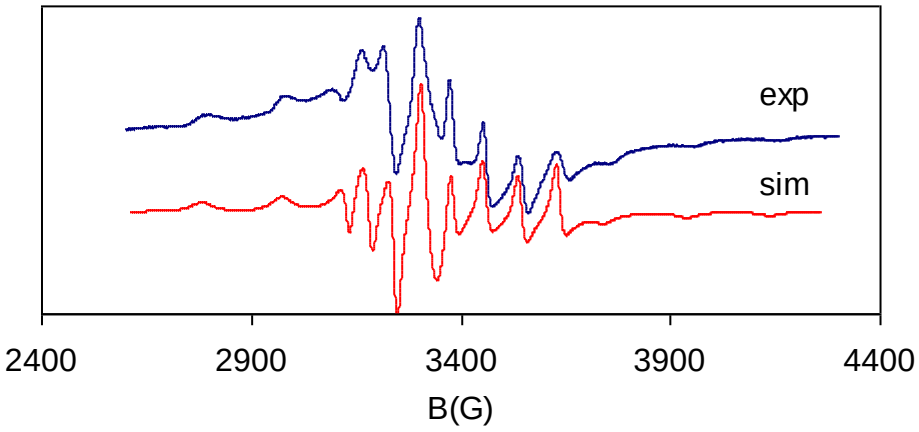

Figure 2

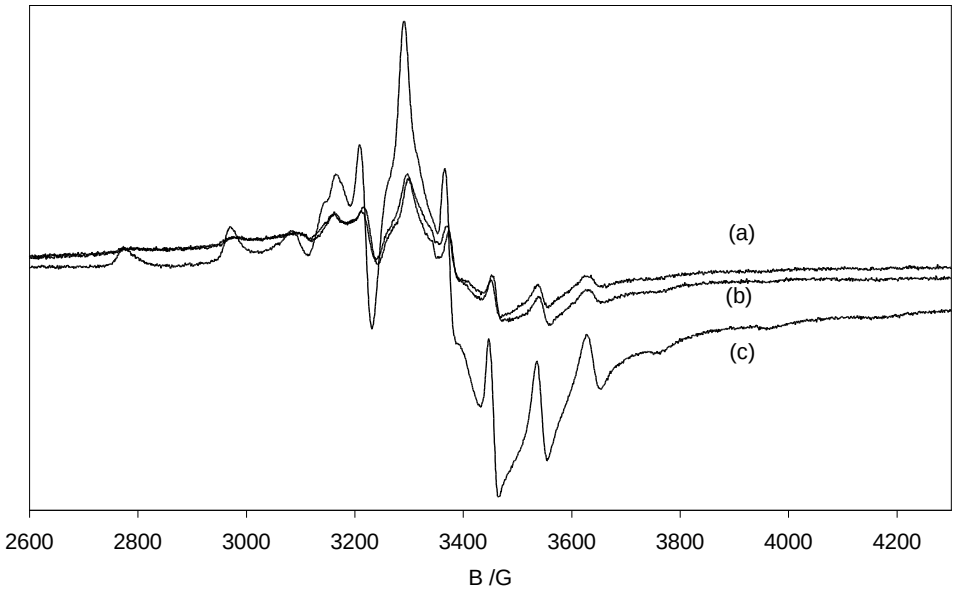

Figure 3

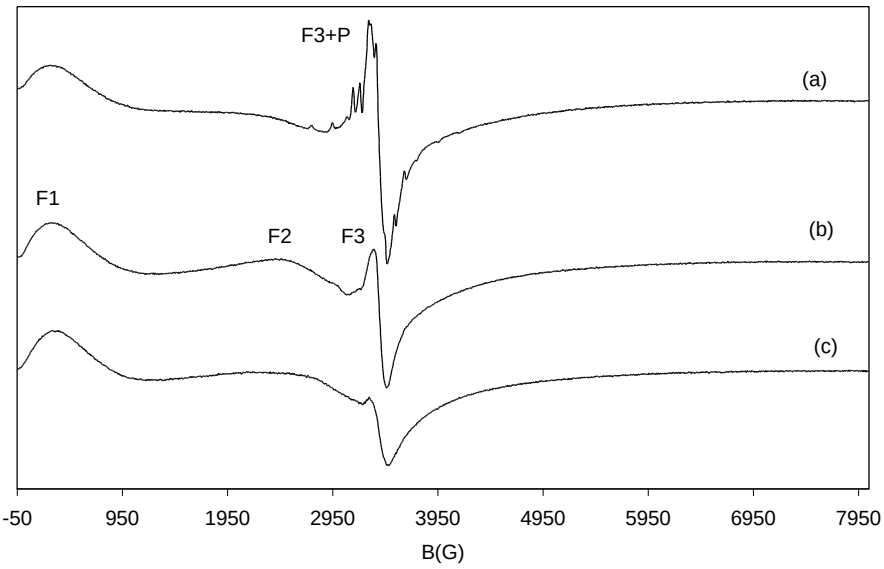

Figure 4

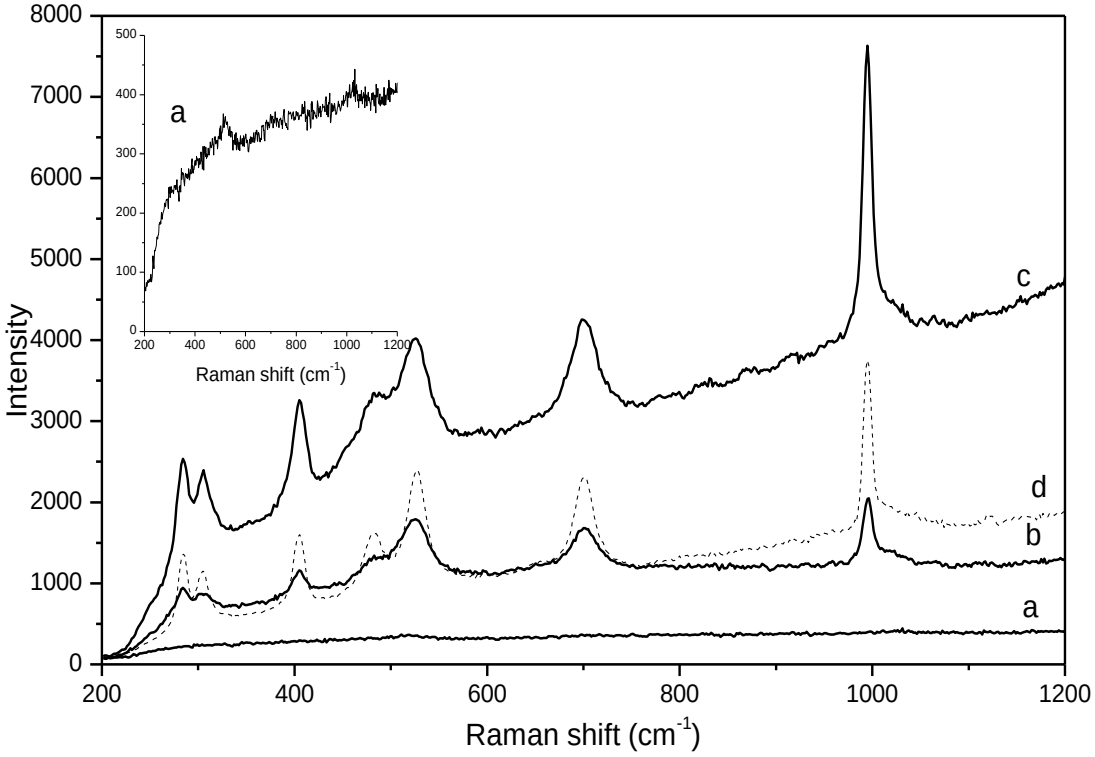

Figure 5

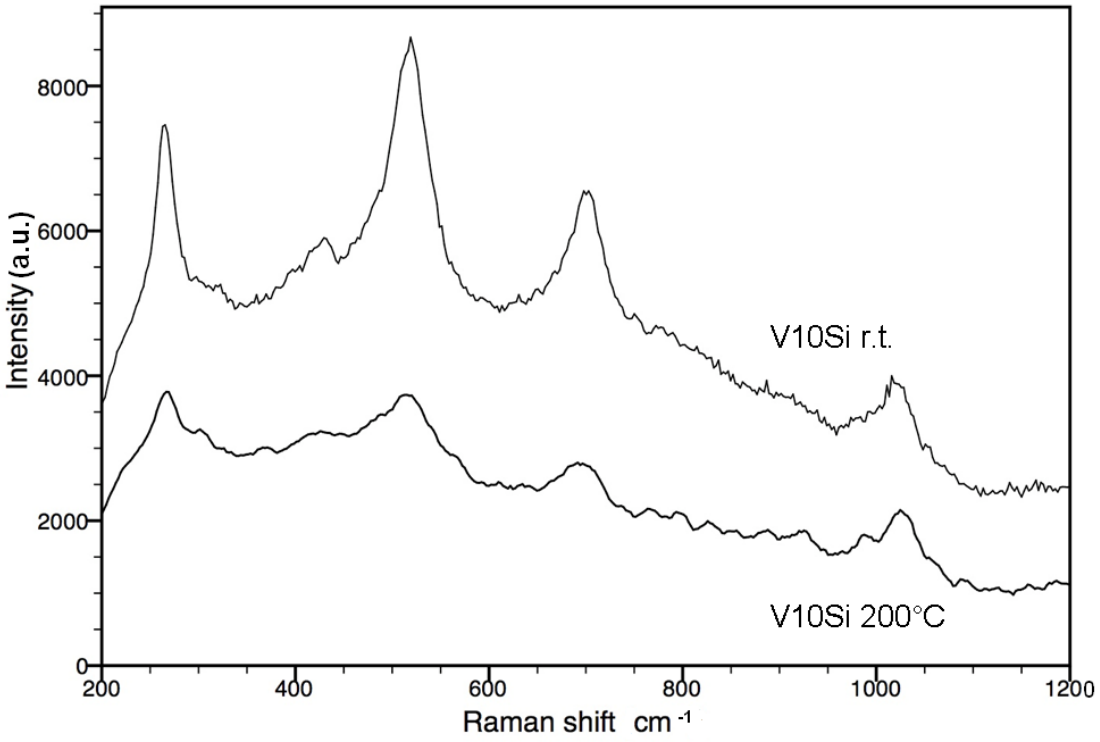
Intensity (a.u.)
8000
6000
4000
2000
0
200
400
600
800
1000
1200
Raman shift cm -1
V10Si r.t.
V10Si 200°C

Figure 6

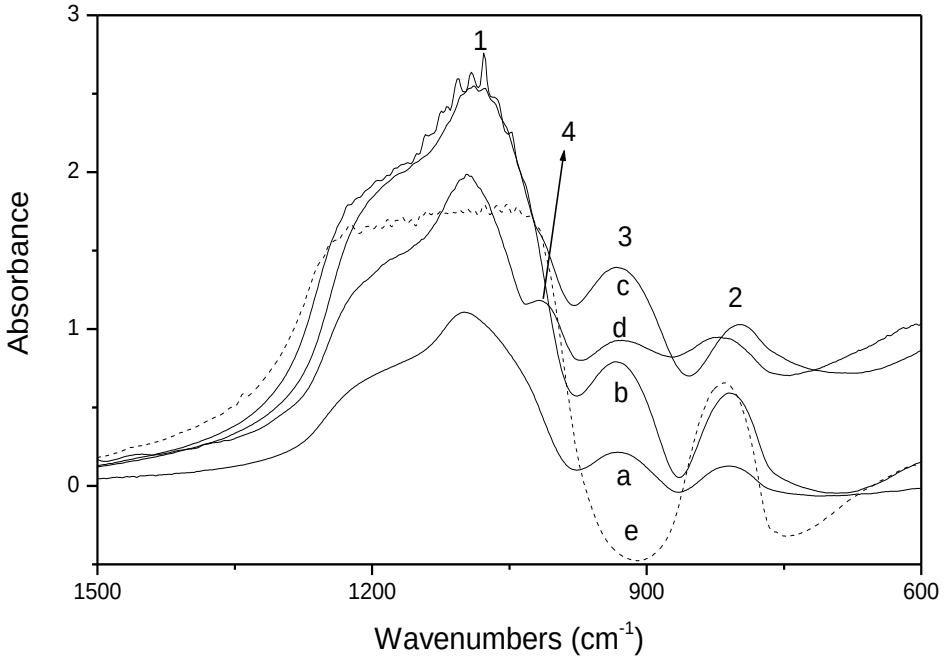
Absorbance
Wavenumbers (cm-1)
1
2
3
4
a
b
c
d
e
0
1
2
3
1500
1200
900
600

Figure 7

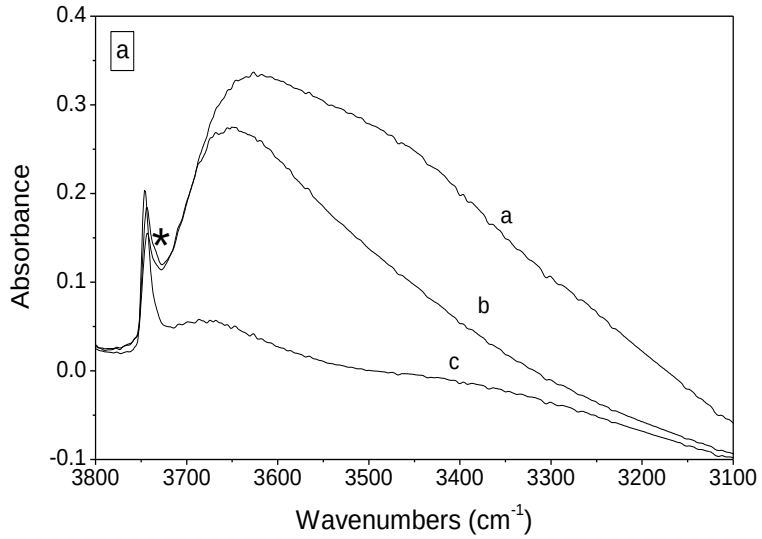

Figure 8*a*

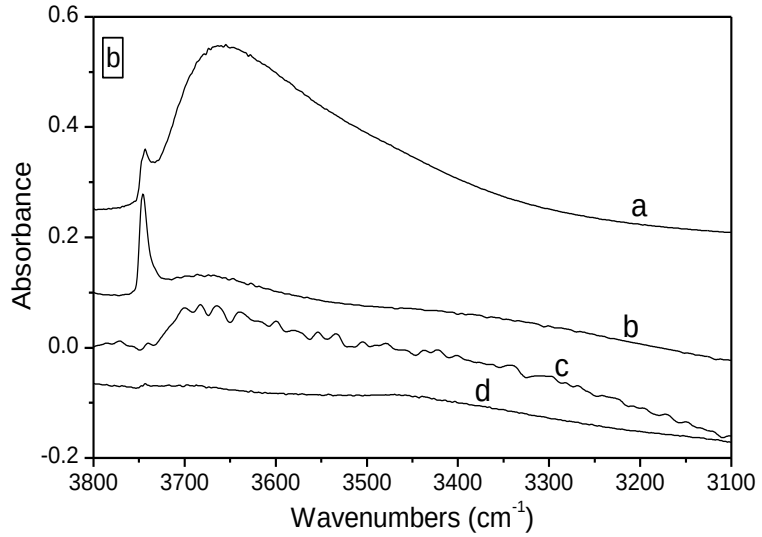

Figure 8*b*

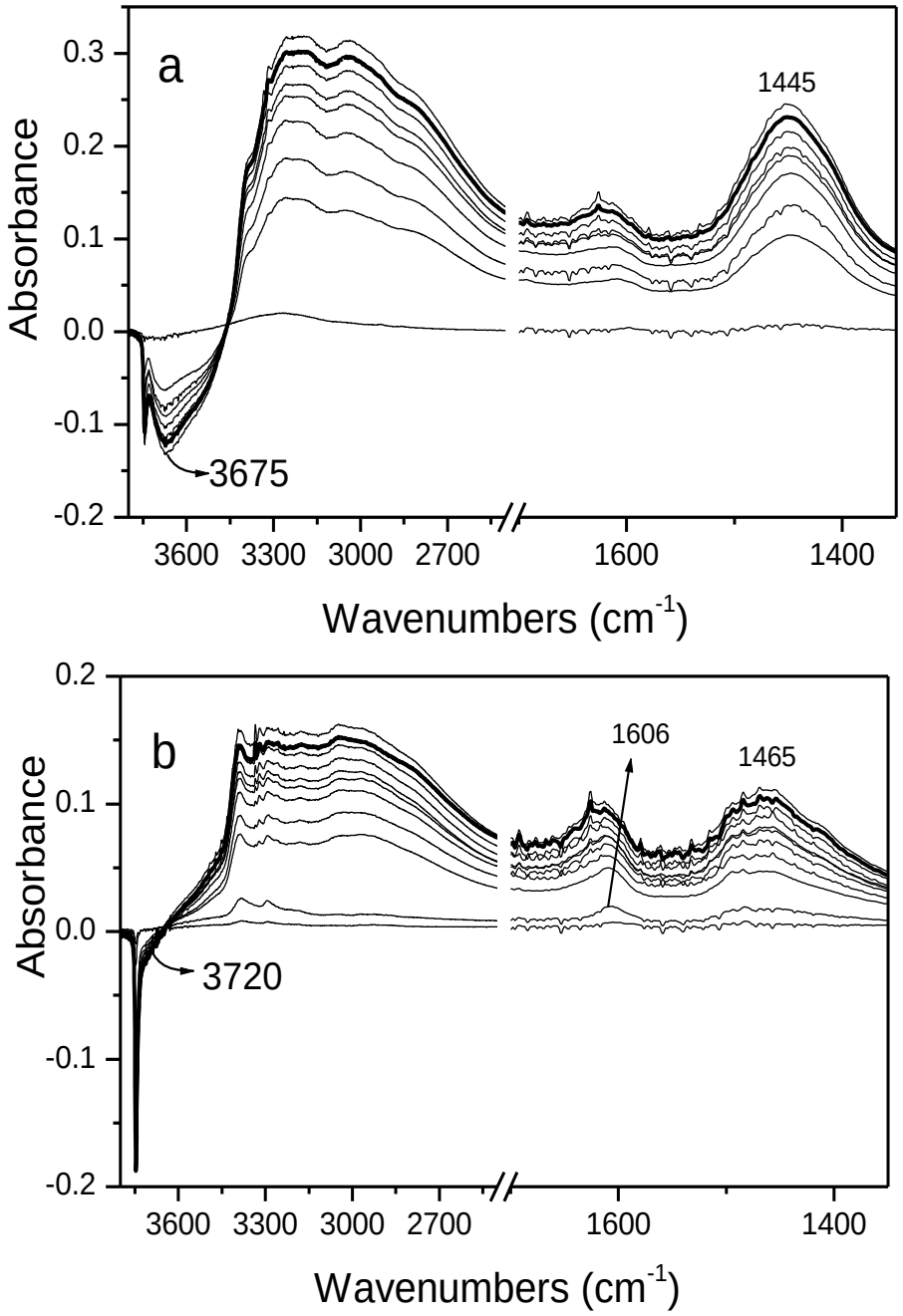
a
1445
3675
Absorbance
0.3
0.2
0.1
0.0
-0.1
-0.2
3600
3300
3000
2700
1600
1400
Wavenumbers (cm-1)
b
1606
1465
3720
Absorbance
0.2
0.1
0.0
-0.1
-0.2
3600
3300
3000
2700
1600
1400
Wavenumbers (cm-1)

Figure 9

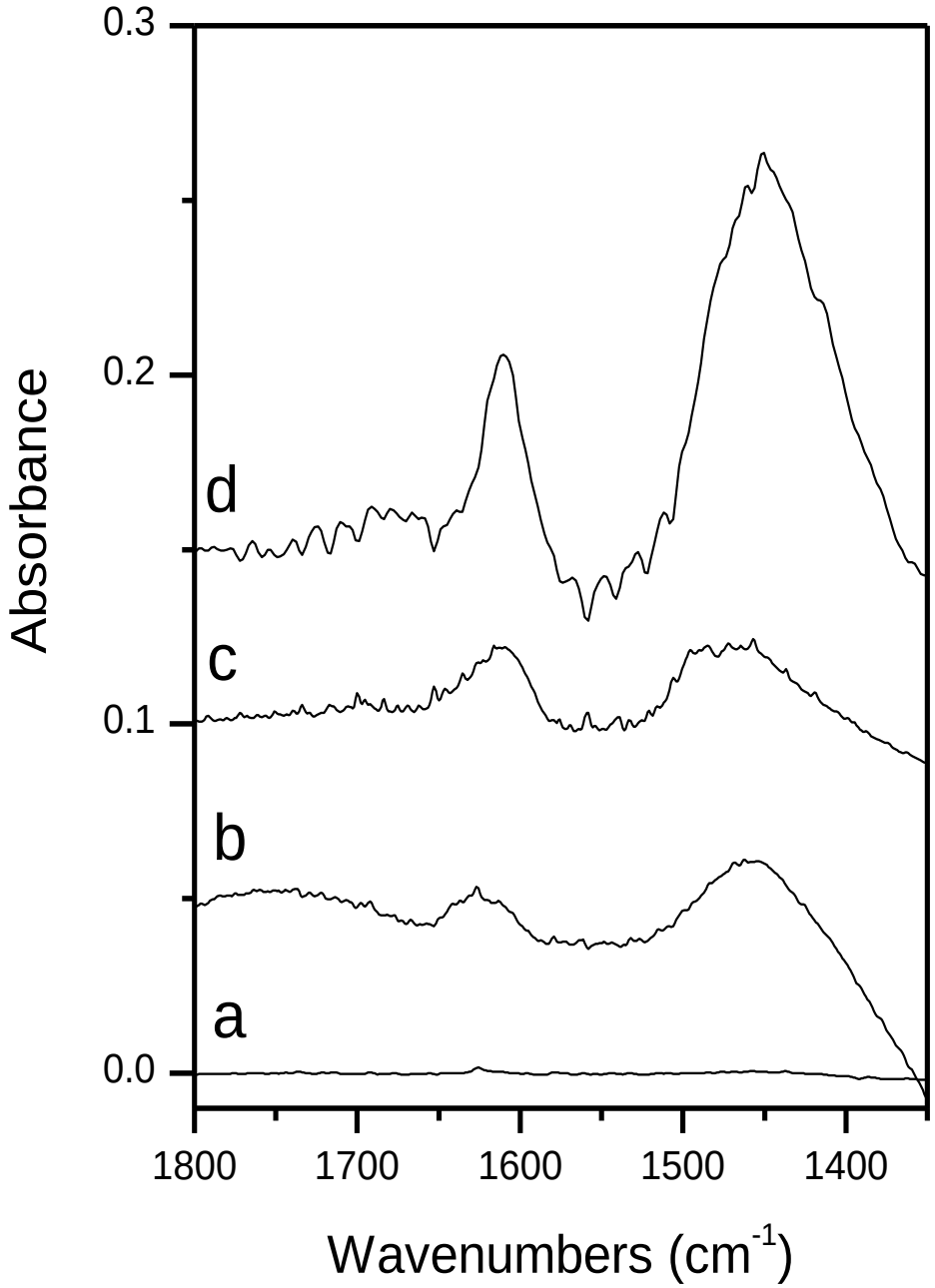
0.3
0.2
0.1
0.0
Absorbance
d
c
b
a
1800
1700
1600
1500
1400
Wavenumbers (cm-1)

Figure 10

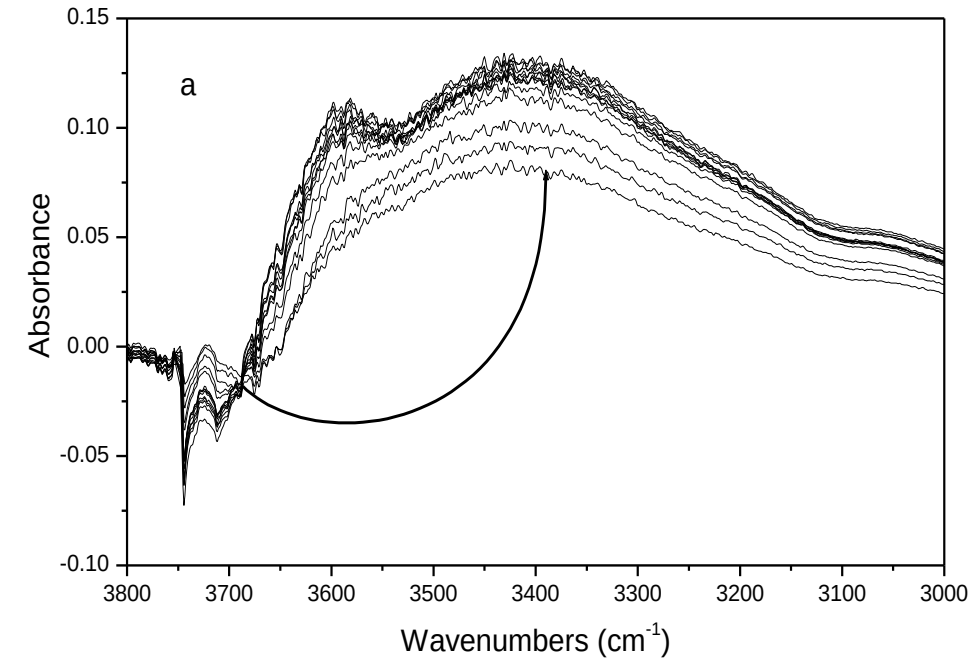
a
Absorbance
0.15
0.10
0.05
0.00
-0.05
-0.10
3800
3700
3600
3500
3400
3300
3200
3100
3000
Wavenumbers (cm-1)

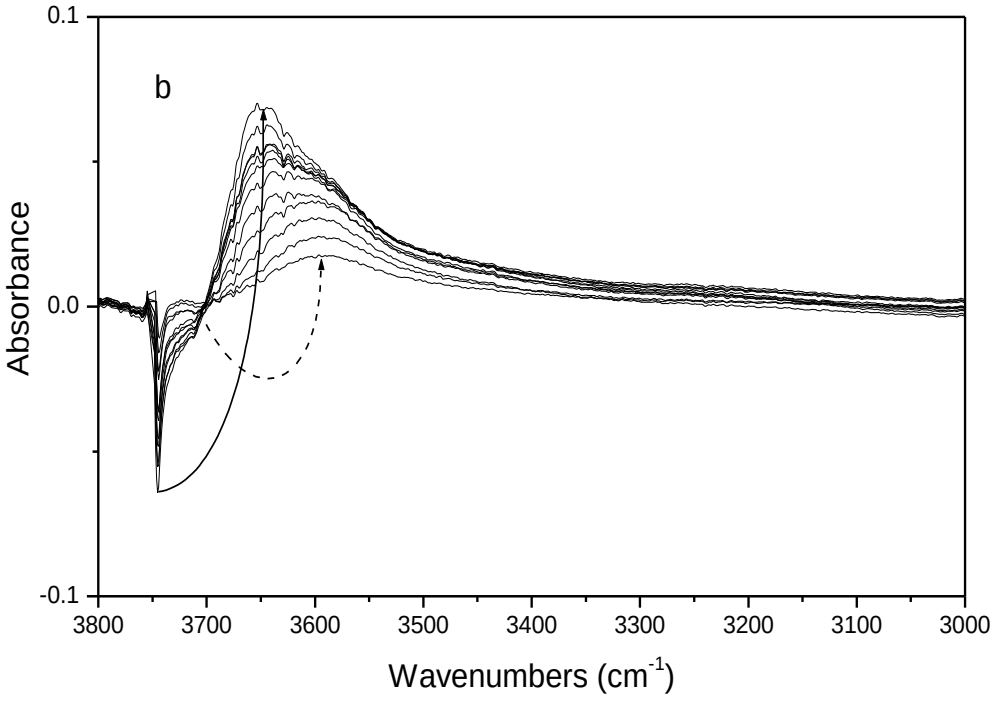
b
Absorbance
0.1
0.0
-0.1
3800
3700
3600
3500
3400
3300
3200
3100
3000
Wavenumbers (cm-1)

Figure 11

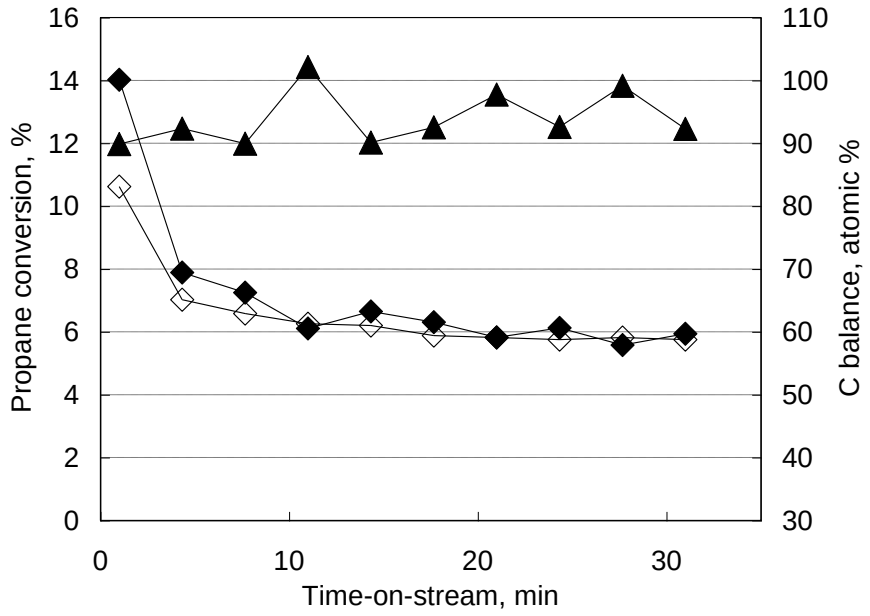

Figure 12*a*

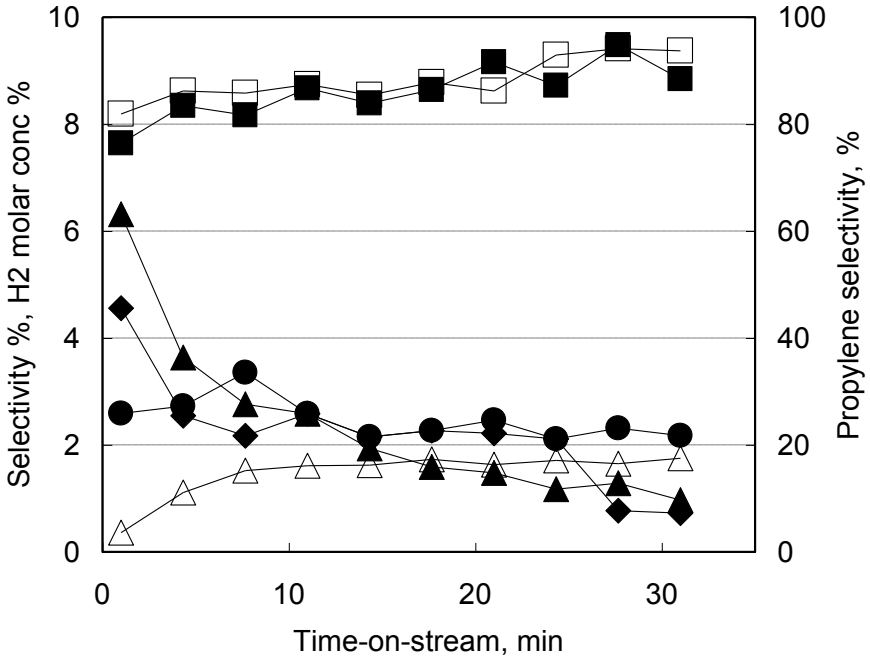

Figure 12*b*

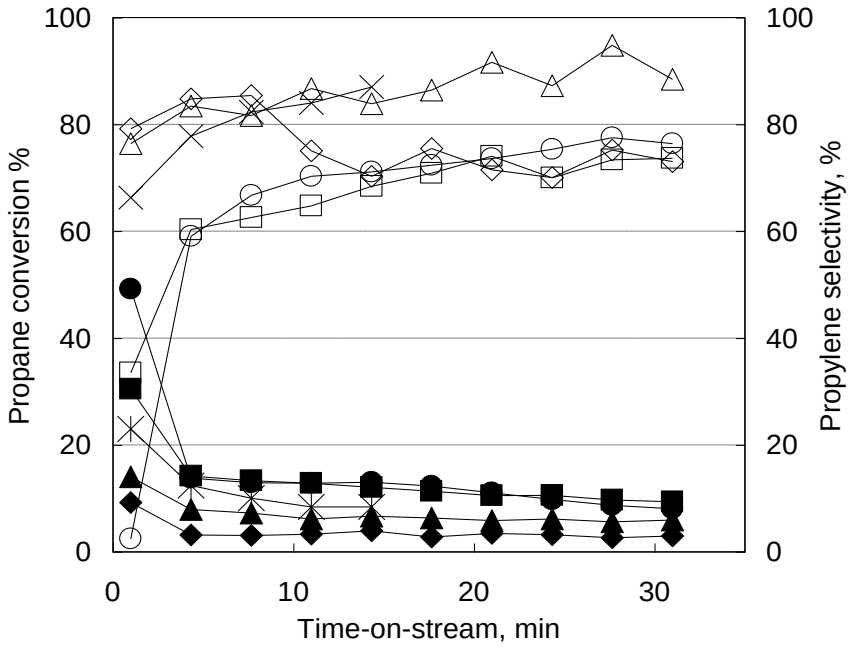
100
80
60
40
20
0
Propane conversion %
Propylene selectivity, %
0
10
20
30
Time-on-stream, min

Figure 12c

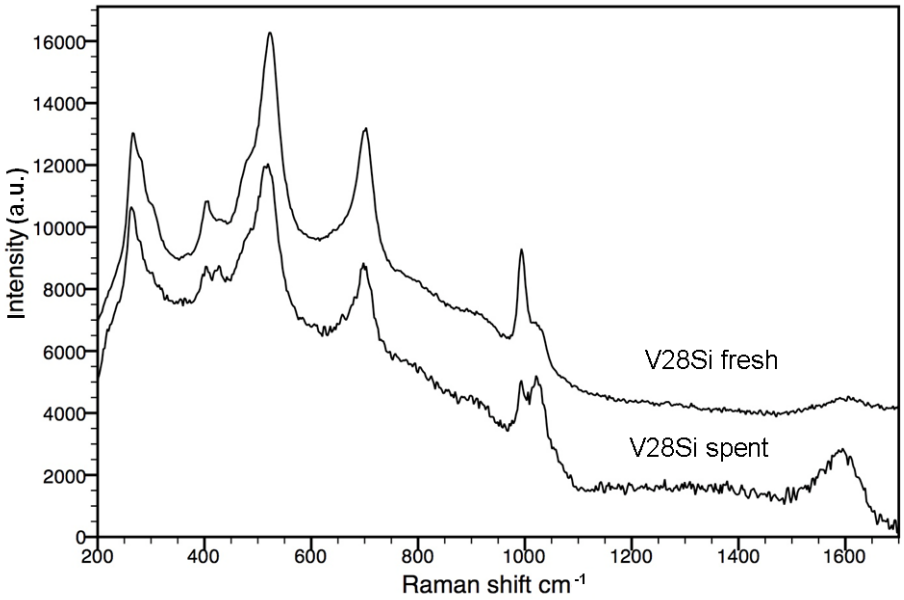
Intensity (a.u.)
16000
14000
12000
10000
8000
6000
4000
2000
0
200
400
600
800
1000
1200
1400
1600
Raman shift cm-1
V28Si fresh
V28Si spent

Figure 13

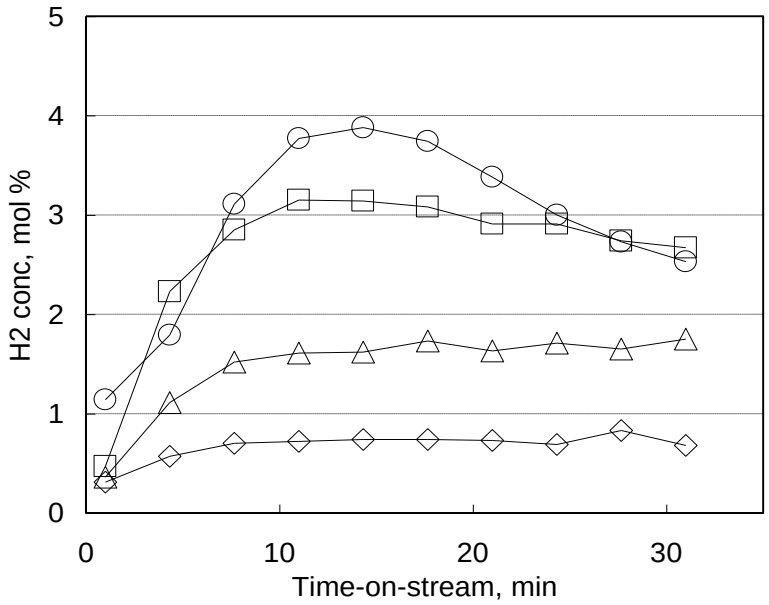

Figure 14a

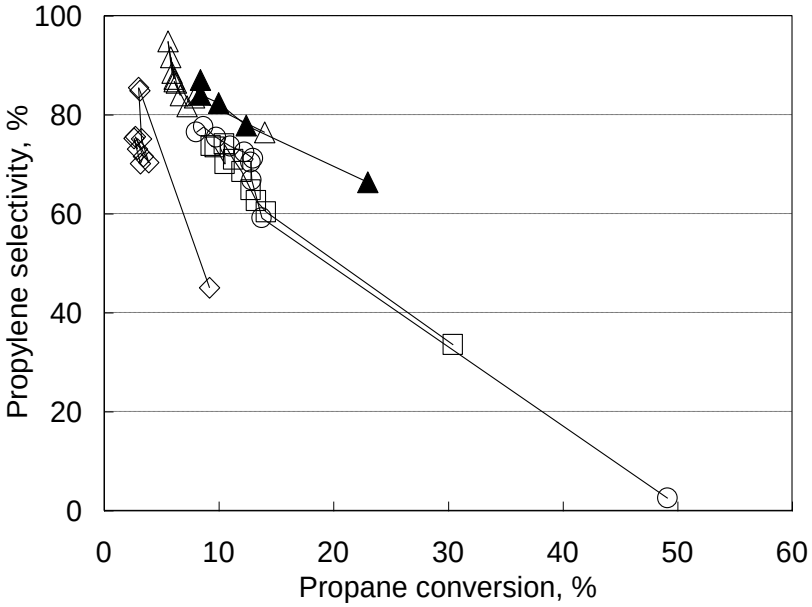

Figure 14b

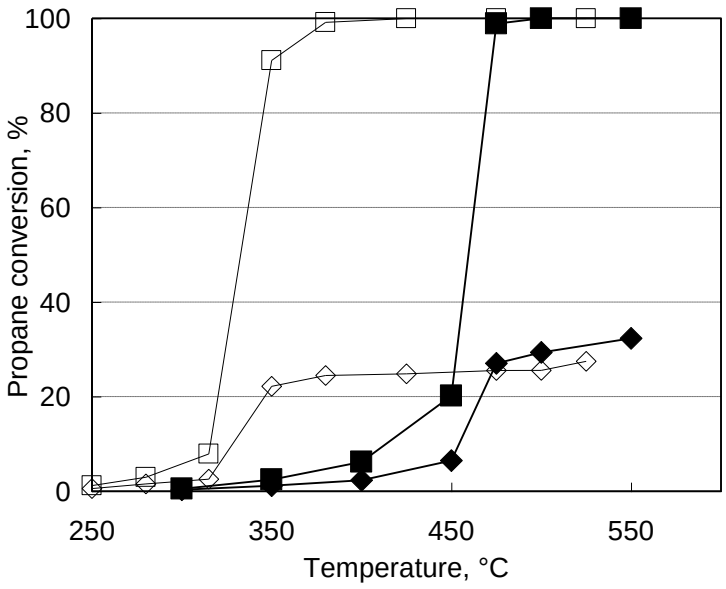

Figure 15a

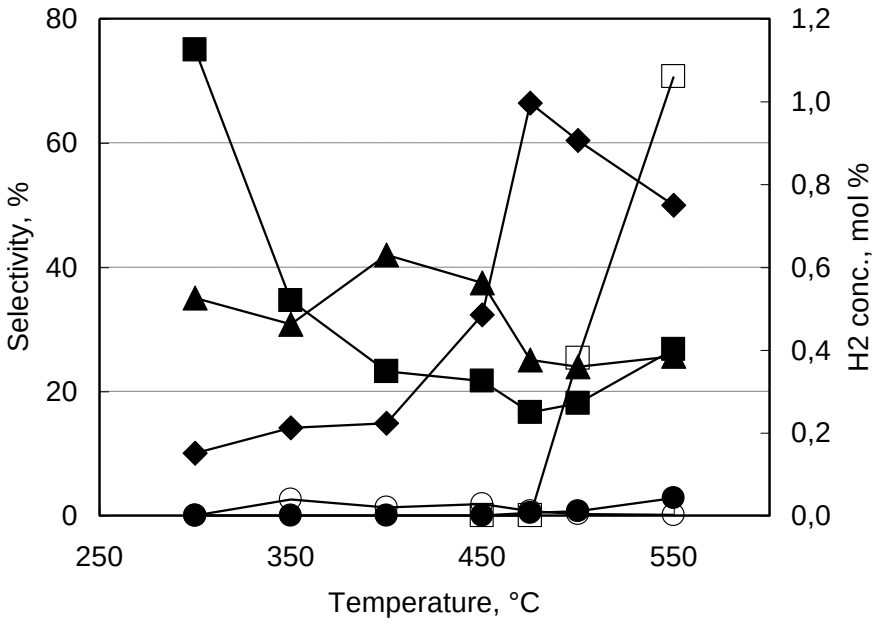

Figure 15b

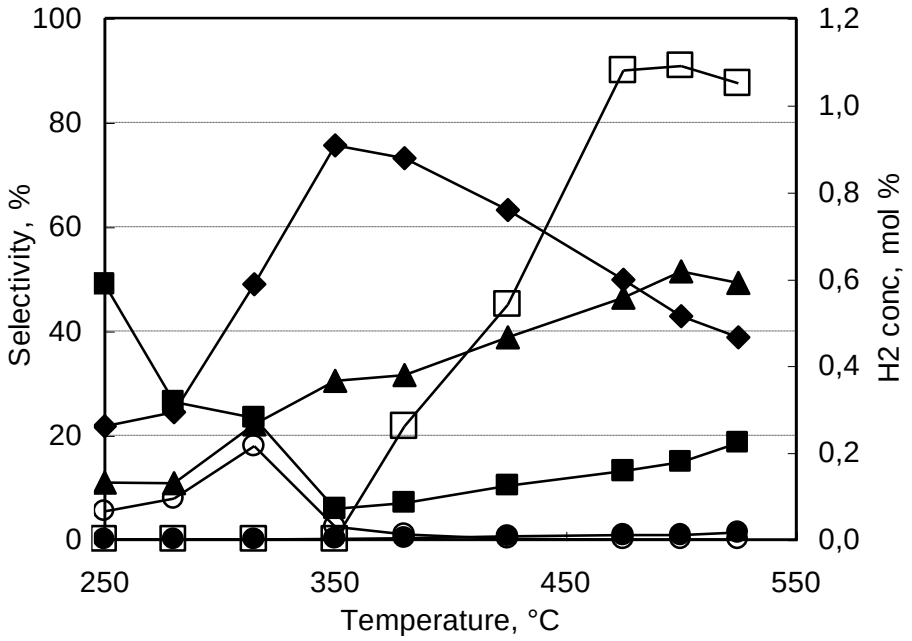
100
80
60
40
20
0
Selectivity, %
1,2
1,0
0,8
0,6
0,4
0,2
0,0
H2 conc, mol %
250
350
450
550
Temperature, °C

Figure 15c

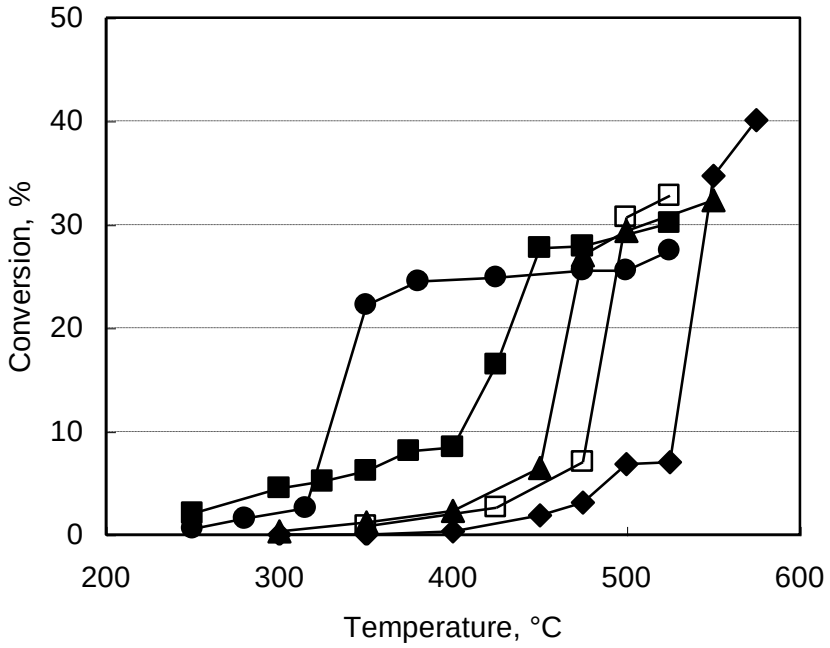

Figure 16*a*

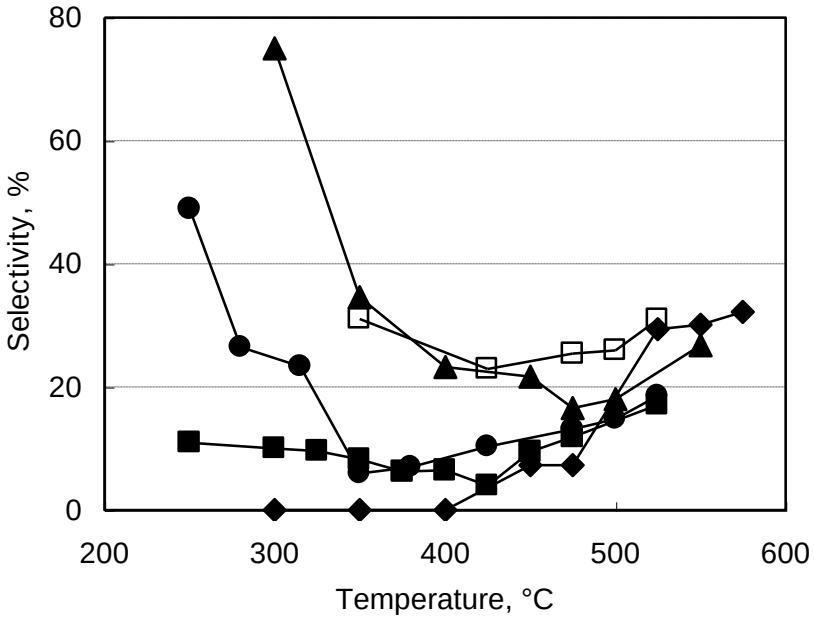

Figure 16*b*

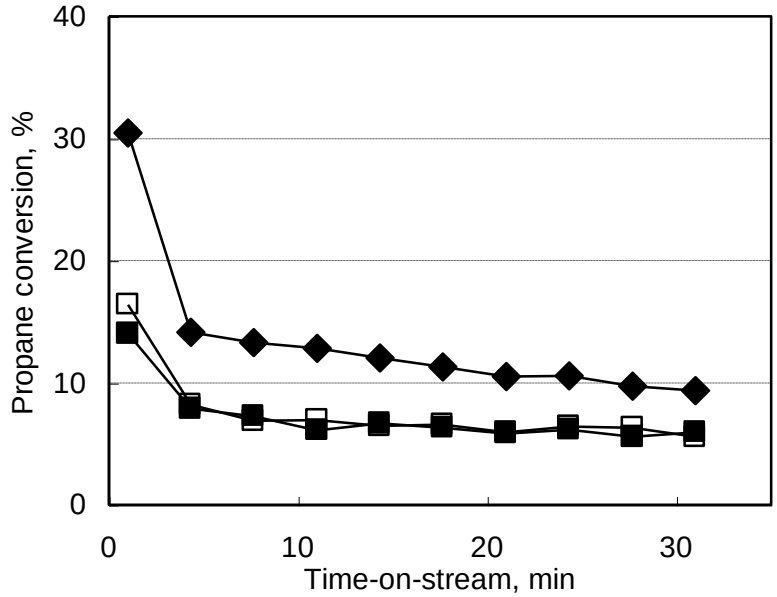

Figure 17*a*

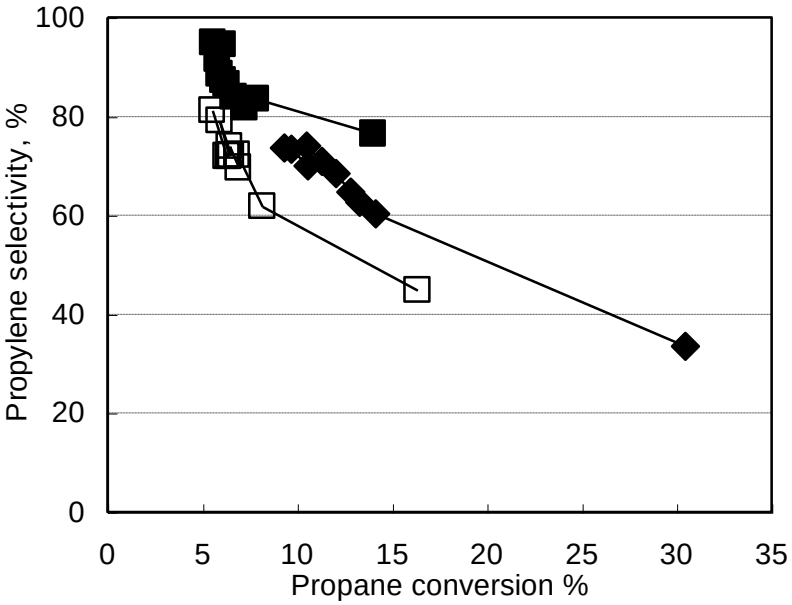

Figure 17*b*

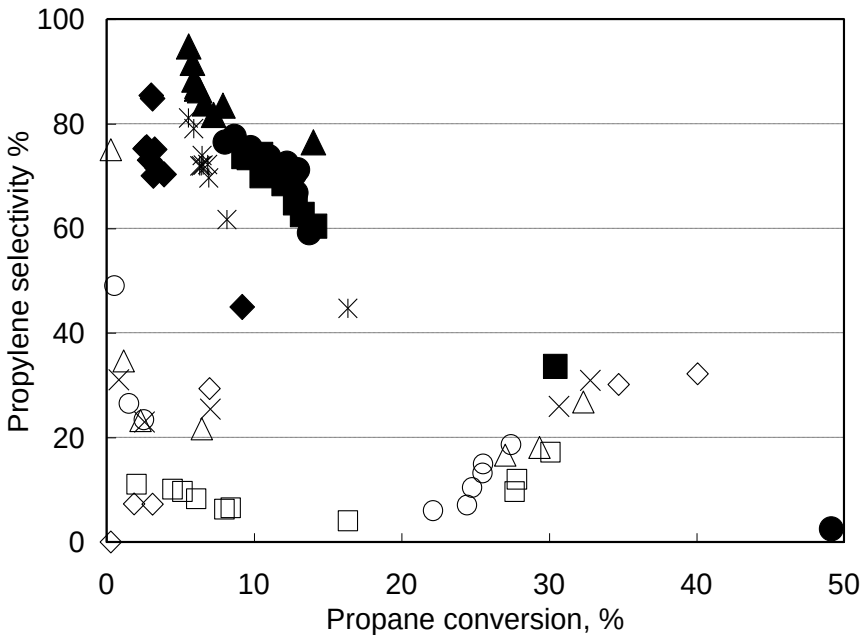
100
80
60
40
20
0
Propylene selectivity %
0
10
20
30
40
50
Propane conversion, %

Figure 18